# Coupled-channels analysis of pion and $\eta$ electroproduction within the Jülich-Bonn-Washington model

M. Mai,[1] M. Döring,[1,2] C. Granados,[1] H. Haberzettl,[1] J. Hergenrather,[1]
Ulf-G. Meißner,[3,4,5] D. Rönchen,[4] I. Strakovsky,[1] and R. Workman[1]
(Jülich-Bonn-Washington Collaboration)

[1]*Institute for Nuclear Studies and Department of Physics, The George Washington University, Washington, DC 20052, USA*
[2]*Thomas Jefferson National Accelerator Facility, Newport News, Virginia 23606, USA*
[3]*Helmholtz-Institut für Strahlen- und Kernphysik (Theorie) and Bethe Center for Theoretical Physics, Universität Bonn, 53115 Bonn, Germany*
[4]*Institute for Advanced Simulation and Jülich Center for Hadron Physics, Forschungszentrum Jülich, 52425 Jülich, Germany*
[5]*Tbilisi State University, 0186 Tbilisi, Georgia*

(Received 17 November 2021; accepted 1 June 2022; published 1 July 2022)

Pion and $\eta$ electroproduction data are jointly analyzed for the first time, up to a center-of-mass energy of 1.6 GeV. The framework is a dynamical coupled-channels model, based on the recent Jülich-Bonn-Washington analysis of pion electroproduction data for the same energy range. Comparisons are made to a number of single-channel $\eta$ electroproduction fits. By comparing multipoles of comparable fit quality, we find some of these amplitudes are well determined over the near-threshold region, while others will require fits over an extended energy range.

DOI: 10.1103/PhysRevC.106.015201

## I. INTRODUCTION

Early progress in baryon spectroscopy was driven by the analysis of meson-nucleon scattering ($\pi N \to \pi N$, $\pi N \to \pi\pi N$); see, e.g., Refs [1–5]. A viable alternative to this, specifically advantageous for detecting unstable intermediate states with small branching ratios to the $\pi N$ channel, is the study of photon-induced reactions [6]. Large databases have been accumulated for these reactions as part of the extensive experimental programs at Jefferson Laboratory, MAMI, ELSA, and other facilities [7–18].

On the theory side, many approaches have been developed to describe these reactions. Specifically for pion electroproduction, chiral perturbation theory (ChPT) has been successfully applied in the analysis of the threshold region [19–23]. In building on ChPT, chiral unitary models (see, e.g., the recent review [24]) have also become quite successful in accessing the resonance region. Such models provide the hadronic structure of many gauge-invariant chiral unitary formalisms [25–31]. For an in-depth discussion of the manifest implementation of gauge invariance see Ref. [32]. For even larger kinematical ranges, and large databases, many phenomenological models have been developed. Major classes of those are (1) isobar models [33–36] with unitarity constraints at lower energies and (2) $K$-matrix-based formalisms with built-in cuts, associated with opening inelastic channels, and dispersion-relation constraints [34,37,38]. Multichannel analyses have analyzed data and, in some cases, amplitudes from hadronic scattering data together with the photon-induced channels [39] by the Gießen [40], Bonn-Gatchina [41], Kent State [5], ANL-Osaka [42], Jülich-Bonn (JüBo) [43], and JPAC [44] groups. For more details, see Ref. [45] and a recent review on baryon spectroscopy [46].

Dynamical coupled-channel approaches [42,43,47–51] (DCC) have led to the discovery and confirmation of many new states [52] by extracting universal resonance parameters in terms of pole positions and residues of the transition amplitude in the complex-energy plane. In many analyses of pion- and photon-induced reactions, mass scans and $\chi^2$ arguments are used to identify new states [53,54], but recently model selection has also been explored [55,56].

Furthermore, by extracting [7,33,35,57–79] the $Q^2$ dependence of resonance couplings, a link between perturbative QCD and the region where quark confinement sets in can be established that serves as point of comparison for many quark models [80–91] and Dyson-Schwinger equations [92–107] (see Ref. [108] for a recent review).

However, so far, no unified coupled-channels analysis of photo- and electroproduction experiments exists that simultaneously describes the $\pi N$, $\eta N$, and $K\Lambda$ final states. The present study provides a first step in this direction in the form of a coupled-channels analysis of pion and $\eta$ electroproduction data, extending our recent analysis of pion electroproduction data [45]. It is based on the JüBo approach [43], which fits an extensive scattering and photoproduction database in the resonance region.

This study is organized as follows. Section II outlines formal aspects of the Jülich-Bonn-Washington (JBW) approach to pseudoscalar meson electroproduction. These include the

 

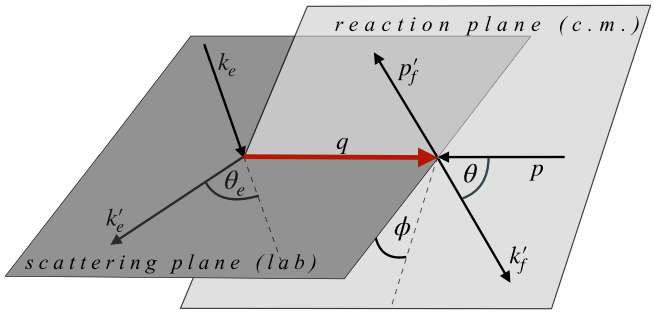


FIG. 1. Kinematics of an electroproduction experiment with the final meson-baryon state $i$. The scattering plane is defined by the respective incoming (outgoing) electron momenta $k_e$ ($k'_e$) with the electron scattering angle $\theta_e$. The reaction plane is spanned by the virtual photon and the outgoing meson, scattered by an angle $\theta$. The momenta $q$ and $p$ correspond to the virtual photon and target nucleon while $k'_f$ and $p'_f$ correspond to the outgoing meson and baryon respectively.

generalization to electroproduction of different final states and the influence of kinematic limits ($Q^2 = 0$, thresholds for channel openings, and pseudothresholds associated with Siegert's theorem [109,110]). Furthermore, we define the parametrization of the $Q^2$ dependence from the photon point at $Q^2 = 0$, where the underlying JüBo model describes photon- and meson-induced reactions, to electroproduction.

Section III reviews the results of previous single-channel fits to $\eta$ electroproduction data. Section IV describes the data used in our fits, strategies to find $\chi^2$ minima, and a modified $\chi^2$ which more evenly weights the contributions of observables with different abundances. Section V compares our fits to data. Eta electroproduction multipoles are also compared, with etaMAID results displayed for reference.

Section VI compares the single- and coupled-channels results, with qualitative features discussed based on data quality and consistency. Finally, prospects for expanded analyses are considered.

## II. FORMALISM

The presentation of the formalism outlined in the following closely follows Ref. [45], but here we generalize the framework to any final meson-baryon state. The multichannel meson electroproduction process in question reads

$$\gamma^*(\boldsymbol{q}) + p(\boldsymbol{p}) \to M(\boldsymbol{k}'_f) + B(\boldsymbol{p}'_f), \tag{2.1}$$

where bold symbols denote three-momenta throughout the paper. The meson and baryon in the final state, with the index $f$, are denoted by $M$ and $B$, respectively. As shown in Fig. 1, the process occurs in two steps, with a virtual photon $\gamma^*(\boldsymbol{q})$ being produced via $e_{\rm in}(\boldsymbol{k}_e) \to e_{\rm out}(\boldsymbol{k}'_e) + \gamma^*(\boldsymbol{q})$, which then scatters off of the proton to a final meson-baryon state. The momentum transfer $Q^2 = -\omega^2 + \boldsymbol{q}^2$, where $\omega$ is the photon energy, is non-negative for spacelike processes, and acts as an independent kinematical variable in addition to the total energy in the center-of-mass (c.m.) frame, $W$. In this frame, the magnitude of the three-momentum of the photon ($q = |\boldsymbol{q}|$) and produced meson ($k' = |\boldsymbol{k}'|$) read

$$q = \frac{\sqrt{\lambda\left(W^2, m_p^2, -Q^2\right)}}{2W}, \quad k'_f = \frac{\sqrt{\lambda\left(W^2, m_f^2, M_f^2\right)}}{2W}, \tag{2.2}$$

where $\lambda(x, y, z) = x^2 + y^2 + z^2 - 2xy - 2yz - 2zx$ denotes the usual Källén triangle function. The meson and baryon masses are denoted throughout this paper by $M_i$ and $m_i$, respectively. With two incoming and three outgoing states there are $(3 + 2) \times 3 - 10 = 5$ independent kinematic variables. The canonical choice for the remaining three (in addition to $W$ and $Q^2$) variables is illustrated in Fig. 1. The quantity $\epsilon = 1 + 2(q_L^2/Q^2)\tan^2\theta_e/2$ contains the electron scattering angle $\theta_e$ and $q_L$ denotes the photon three-momentum in the laboratory frame. The angle of the reaction plane to the scattering plane is given by $\phi$ and $\theta$ is the c.m. meson scattering angle in the latter plane. The experimental data discussed in the Sec. IV are represented with respect to these five variables $\mathcal{O}(Q^2, W, \phi, \theta, \epsilon)$.

As discussed in the previous paper [45] based on the seminal papers [111–114], the process of a photon-induced production of a meson off a nucleon is encoded in the transition amplitude. In the one-photon approximation, and considering the continuity equation for the current, the latter can be expressed in terms of three independent multipoles for a fixed quantum number $\ell_\pm$ of the final meson-baryon state. We chose those to be electric, magnetic and longitudinal multipoles $E_{\ell\pm}(W, Q^2)$, $M_{\ell\pm}(W, Q^2)$ and $L_{\ell\pm}(W, Q^2)$ with the latter related to the often-used Coulomb multipole as $\omega C_{\ell\pm}(W, Q^2) = qL_{\ell\pm}(W, Q^2)$. Each of the introduced multipoles carry a discrete index corresponding to the total angular momentum $J = \ell \pm 1/2$ and final-state index $\mu$, e.g., $E_{0+}^{\eta p}$.

We construct the electroproduction multipoles on the basis of the dynamical coupled-channels Jülich-Bonn (JüBo) approach [49,115] that provides the boundary condition at $Q^2 = 0$, incorporating the experimental information from real-photon and pion-induced reactions. In this approach, two-body unitarity and analyticity are respected and the baryon resonance spectrum is determined in terms of poles in the complex energy plane on the second Riemann sheet [116,117].

Extending the ansatz of the JüBo approach, we begin by introducing a generic function ($\bar{\mathcal{M}}$) for each electromagnetic multipole ($\mathcal{M}_{\mu\gamma^*} \in \{E_\mu, M_\mu, L_\mu\}$) as

$$\begin{aligned}\overline{\mathcal{M}}_{\mu\gamma^*}(k, W, Q^2) = V_{\mu\gamma^*}(k, W, Q^2) \\ + \sum_\kappa \int_0^\infty dp\, p^2\, T_{\mu\kappa}(k, p, W) \\ \times G_\kappa(p, W) V_{\kappa\gamma^*}(p, W, Q^2),\end{aligned} \tag{2.3}$$

where $\mu$ is a channel index and the summation extends over intermediate meson-baryon channels $\kappa \in \{\pi N, \eta N, K\Lambda, K\Sigma, \pi\Delta, \rho N\}$. Note that the $\sigma N$ channel is not part of this list. The $\sigma N$ channel is part of the final-state interaction, but neither the hadronic resonance vertex functions nor the photon are directly coupled to it; once photon or electroproduction data of the $\pi\pi N$ final state are analyzed, such couplings will become relevant and will be

included. Note that we have suppressed isospin and angular momentum index $\ell_\pm$ in Eq. (2.3).

The electroproduction kernel $V_{\mu\gamma^*}$ in Eq. (2.3) is parametrized as

$$V_{\mu\gamma^*}(p,W,Q^2) = \alpha^{NP}_{\mu\gamma^*}(p,W,Q^2) + \sum_{i=1}^{i_{\max}} \frac{\gamma^a_{\mu;i}(p)\gamma^c_{\gamma^*;i}(W,Q^2)}{W-m^b_i}, \tag{2.4}$$

introducing the $Q^2$ dependence via a separable ansatz,

$$\alpha^{NP}_{\mu\gamma^*}(p,W,Q^2) = \tilde{F}_\mu(Q^2)\alpha^{NP}_{\mu\gamma}(p,W),$$
$$\gamma^c_{\gamma^*;i}(W,Q^2) = \tilde{F}_i(Q^2)\gamma^c_{\gamma;i}(W). \tag{2.5}$$

The $Q^2$-independent pieces on the right-hand side of both equations represent the input from the JüBo2017 solution [47]. Specifically, $\gamma^c_{\gamma;i}$ describes the interaction of the photon with the resonance state $i$ with bare mass $m^b_i$ and $\alpha^{NP}_{\mu\gamma}$ accounts for the coupling of the photon to the so-called background or nonpole part of the amplitude. Both quantities are parametrized by energy-dependent polynomials; see Ref. [49].

The $Q^2$ dependence is encoded entirely in the channel-dependent form-factor $\tilde{F}_\mu(Q^2)$ and another channel-independent form-factor $\tilde{F}_i(Q^2)$ that depends on the resonance index $i$. We emphasize that this structure is inherited from the JüBo photoproduction ansatz, which separates the photon-induced vertex ($\gamma^c$) from the decay vertex of a resonance to the final meson-baryon pair ($\gamma^a_\mu$). Both $\tilde{F}_\mu(Q^2)$ and $\tilde{F}_i(Q^2)$ are chosen as

$$\tilde{F}_\mu(Q^2) = \tilde{F}_D(Q^2)\, e^{-\beta^0_\mu Q^2/m^2}\, P^N(Q^2/m^2, \vec{\beta}_\mu),$$
$$\tilde{F}_i(Q^2) = \tilde{F}_D(Q^2)\, e^{-\delta^0_i Q^2/m^2}\, P^N(Q^2/m^2, \vec{\delta}_i), \tag{2.6}$$

where $P^N(x,\vec{y}) = 1 + xy_1 + \cdots + x^N y_N$ is a general polynomial with free parameters to be fitted together with $\delta^0_i$ and $\beta^0_\mu$ to experimental electroproduction data. The parameter-free form factor $\tilde{F}_D(Q^2)$ encodes the empirical dipole behavior, usually implemented in such problems, as well as a Woods-Saxon form factor which ensures suppression at large $Q^2$. It reads

$$\tilde{F}_D(Q^2) = \frac{1}{(1+Q^2/b^2)^2}\,\frac{1+e^{-Q^2_r/Q^2_w}}{1+e^{(Q^2-Q^2_r)/Q^2_w}} \tag{2.7}$$

with $b^2 = 0.71$ GeV$^2$, $Q^2_w = 0.5$ GeV$^2$, and $Q^2_r = 4.0$ GeV$^2$; see Ref. [45] for more details

As stated above, this procedure relies heavily on the input from the photoproduction, i.e., the functions $\alpha^{NP}_{\mu\gamma}(p,W)$ and $\gamma^c_{\gamma;i}(W)$. Obviously, such an input cannot exist for the longitudinal multipoles as their contribution vanishes exactly at the photon point. In this case we employ a strategy similar to that of Ref. [26]:

(1) We recall that at the *pseudothreshold* ($q=0$) the electric and longitudinal multipoles relate according to the Siegert's condition as

$$\left.\frac{E_{\ell+}}{L_{\ell+}}\right|_{q=0} = 1, \quad \left.\frac{E_{\ell-}}{L_{\ell-}}\right|_{q=0} = \frac{\ell}{1-\ell}. \tag{2.8}$$

For more details, see Secs. 2.2 and 2.3 of Ref. [26], or the original derivations in Refs. [110,114]. Therefore, we apply at the nearest pseudothreshold point, $Q^2_{\rm PT} = -(W-m)^2$,

$$\alpha^{NP,L_{\ell\pm}}_{\mu\gamma^*}(p,W,Q^2) = \frac{\omega}{\omega_{\rm PT}}\frac{\tilde{F}_D(Q^2)}{\tilde{F}_D\big(Q^2_{\rm PT}\big)} D^{\ell\pm}_\mu(W,Q^2)\alpha^{NP,E_{\ell\pm}}_{\mu\gamma^*}\big(p,W,Q^2_{\rm PT}\big) \tag{2.9}$$

and

$$\gamma^{c,L_{\ell\pm}}_{\gamma^*;i}(W,Q^2) = \frac{\omega}{\omega_{\rm PT}}\frac{\tilde{F}_D(Q^2)}{\tilde{F}_D\big(Q^2_{\rm PT}\big)} \tilde{D}^{\ell\pm}_i(W,Q^2)\gamma^{c,E_{\ell\pm}}_{\gamma^*;i}\big(W,Q^2_{\rm PT}\big). \tag{2.10}$$

The photon energy is $\omega_{\rm PT} = (W^2 - m^2 - Q^2_{\rm PT})/(2W)$. The new functions $D^{\ell\pm}(Q^2)$ ensure Siegert's condition and consistent falloff behavior in $Q^2$ as

$$D^{\ell+}_\mu(W,Q^2) = e^{-\beta^0_\mu q/q_\gamma}\, P^N(q/q_\gamma, \vec{\beta}_\mu),$$
$$\tilde{D}^{\ell+}_i(W,Q^2) = e^{-\delta^0_i q/q_\gamma}\, P^N(q/q_\gamma, \vec{\delta}_i),$$
$$D^{\ell-}_\mu(W,Q^2) = -\frac{\ell-1}{\ell} e^{-\beta^0_i q/q_\gamma}\, P^N(q/q_\gamma, \vec{\beta}_\mu),$$
$$\tilde{D}^{\ell-}_i(W,Q^2) = -\frac{\ell-1}{\ell} e^{-\delta^0_i q/q_\gamma}\, P^N(q/q_\gamma, \vec{\delta}_i), \tag{2.11}$$

respectively to the pole and nonpole parts for $q_\gamma = q(Q^2=0)$.

(2) In two specific cases $[(\ell\pm, I) = (1-, 1/2)$ and $(\ell\pm, I) = (1-, 3/2)]$ the electric multipole vanishes due to selection rules, rendering the implementation of Siegert's theorem nonsensical. In these cases, we obtain the longitudinal multipole from the magnetic one using a new real-valued normalization constants $\zeta^{NP}$ to be determined from the fit,

$$\alpha^{NP,L_{\ell\pm}}_{\mu\gamma^*}(p,W,Q^2) = \zeta^{NP}_\mu \frac{\omega}{\omega_{\rm PT}}\tilde{F}^\mu(Q^2)\alpha^{NP,M_{\ell\pm}}_{\mu\gamma^*}(p,W),$$
$$\gamma^{c,L_{\ell\pm}}_{\gamma^*;i}(W,Q^2) = \zeta_i \frac{\omega}{\omega_{\rm PT}}\tilde{F}^\mu(Q^2)\gamma^{c,M_{\ell\pm}}_{\gamma;i}(W). \tag{2.12}$$

Before writing down the final relation between the generic multipole functions ($\bar{E}_{\ell\pm}$, $\bar{M}_{\ell\pm}$, $\bar{L}_{\ell\pm}$) and corresponding multipoles, we note that the latter obey a certain behavior at the pseudothreshold ($q=0$) and production threshold ($k=0$),

$$\ell \geqslant 0: \quad \lim_{k\to0} E_{\ell+} = k^\ell, \quad \lim_{q\to0} E_{\ell+} = q^\ell,$$
$$\ell \geqslant 0: \quad \lim_{k\to0} L_{\ell+} = k^\ell, \quad \lim_{q\to0} L_{\ell+} = q^\ell,$$
$$\lim_{k\to0} L_{1-} = k, \quad \lim_{q\to0} L_{1-} = q,$$
$$\ell \geqslant 1: \quad \lim_{k\to0} M_{\ell\pm} = k^\ell, \quad \lim_{q\to0} M_{\ell\pm} = q^\ell,$$

$$\ell \geqslant 2: \quad \lim_{k\to 0} E_{\ell-} = k^{\ell}, \quad \lim_{q\to 0} E_{\ell-} = q^{\ell-2},$$
$$\ell \geqslant 2: \quad \lim_{k\to 0} L_{\ell-} = k^{\ell}, \quad \lim_{q\to 0} L_{\ell-} = q^{\ell-2}. \quad (2.13)$$

We incorporate these conditions using

$$\mathcal{M}_{\mu\gamma^*}(k, W, Q^2) = R_{\ell'}(\lambda, q/q_\gamma)\overline{\mathcal{M}}_{\mu\gamma^*}(k, W, Q^2) \quad (2.14)$$

for each multipole type and total angular momentum individually. Here,

$$R_{\ell'}(\lambda, r) = \frac{B_{\ell'}(\lambda r)}{B_{\ell'}(\lambda)} \quad \text{with}$$
$$\ell' = \begin{cases} \ell & \text{for } E_{\ell+}, L_{\ell\pm}, M_{\ell\pm}, \\ \ell - 2 & \text{for } E_{\ell-}, L_{\ell-}, \text{ and } \ell \geqslant 2, \end{cases} \quad (2.15)$$

using Blatt-Weisskopf barrier-penetration factors [118,119],

$$B_0(r) = 1,$$
$$B_1(r) = r/\sqrt{1+r^2},$$
$$B_2(r) = r^2/\sqrt{9+3r^2+r^4},$$
$$B_3(r) = r^3/\sqrt{225+45r^2+6r^4+r^6},$$
$$B_4(r) = r^4/\sqrt{11025+1575r^2+135r^4+10r^6+r^8}. \quad (2.16)$$

New free parameters $\lambda$ need to be determined from a fit to experimental data. For simplicity and to keep the number of parameters low, the $\lambda$'s are chosen as channel independent.

In summary, for every partial wave, the multipoles $E_{\mu\gamma^*}$, $M_{\mu\gamma^*}$, and $L_{\mu\gamma^*}$ are fully determined up to (1) $(1+N)$ channel-dependent fit parameters $\beta_\mu^0, \ldots, \beta_\mu^N$ for the nonpole part; (2) $(1+N)$ channel-independent parameters $\delta_i^0, \ldots, \delta_i^N$ for each of the $i_{\max}$ resonances; (3) one channel-independent threshold behavior regulating parameter $\lambda$; (4) channel-(in)dependent normalization factors $\zeta_\mu^{NP}(\zeta_i)$. Finally, any observable can be constructed from the described multipoles using a standard procedure involving CGLN (Chew, Goldberger, Low, and Nambu) and helicity amplitudes [111]. For explicit formulas we refer the reader to the previous publication [45].

## III. PREVIOUS SINGLE-CHANNEL FITS

Before discussing our findings for the coupled-channels case, we review what has been learned from fits to the $\eta$ electroproduction data alone. The etaMAID model [33] is similar to the MAID2007 analysis [35] of pion production, with the fit including both $\eta$ photo- and electroproduction data. It differs from MAID2007 by a phase factor which was adjusted to the corresponding pion-nucleon phase. For $\eta$ photo- and electroproduction this was not found to be feasible, due to the quality and range of available $\eta N$ production data. As a result, there exists an overall phase ambiguity, in comparisons of

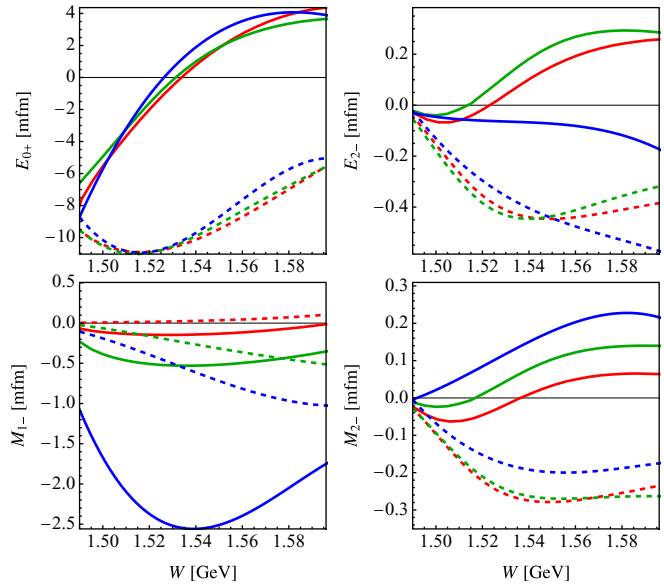


FIG. 2. Selected $\eta$ photoproduction multipoles in the isospin basis from JüBo [47] (blue), etaMAID [33] (red), and Bonn-Gatchina [120] (green) approaches. Real and imaginary parts are depicted by full and dashed lines, respectively. A phase factor $(-1)$ is applied to the etaMAID solution.

different $\eta$ photoproduction fits, which cannot be determined experimentally. Comparing the $\eta$ photoproduction fits of etaMAID and the Jülich-Bonn approach, overall qualitative agreement is improved by applying a simple overall sign. This is illustrated in Fig. 2. The overall phase, applied to etaMAID, yeilds a quantitative agreement between the JüBo, etaMAID, and Bonn-Gatchina determinations of the $E_{0+}$ multipole. The $M_{2-}$ multipole shows qualitative agreement, while the $M_{1-}$ and $E_{2-}$ multipoles show differences in sign and scale that hinder a comparison of electroproduction results extrapolated to $Q^2 = 0$.

The $\eta$ electroproduction fit of etaMAID requires a determination of the $Q^2$ dependence, which is chosen to be simpler than what was used for pion electroproduction (MAID2007). The dominant $S$-wave multipole near threshold, in principle, includes both the $N(1535)$ and $N(1650)$ resonance contributions. These have been combined using a single-quark transition model [170]. For the $N(1535)$ multipole, the $Q^2$ dependence is assumed to be proportional to a dipole form factor multiplied by a ratio of linear functions of $Q^2$. Other resonance multipoles have $Q^2$ dependence approximated by a simple dipole factor multiplied by a ratio of kinematic factors.

Included in etaMAID are the above mentioned $N(1535)$ and $N(1650)$, together with the $N(1520)$, $N(1675)$, $N(1700)$, $N(1710)$, and $N(1720)$. Of these, the $N(1650)$, $N(1675)$, $N(1710)$, and $N(1720)$ were found to have $\eta N$ branching ratios at the 3–26% level; the $N(1520)$, $N(1680)$, and $N(1700)$ contributed with branching ratios less than 1%. The $N(1535)$ had a 50% branching to the $\eta N$ channel; the Review of Particle Properties [52] gives an estimate of 30–55% for this quantity. Included in the fit were data available as of 2001, the cross section measurements of Refs. [167] and [169].

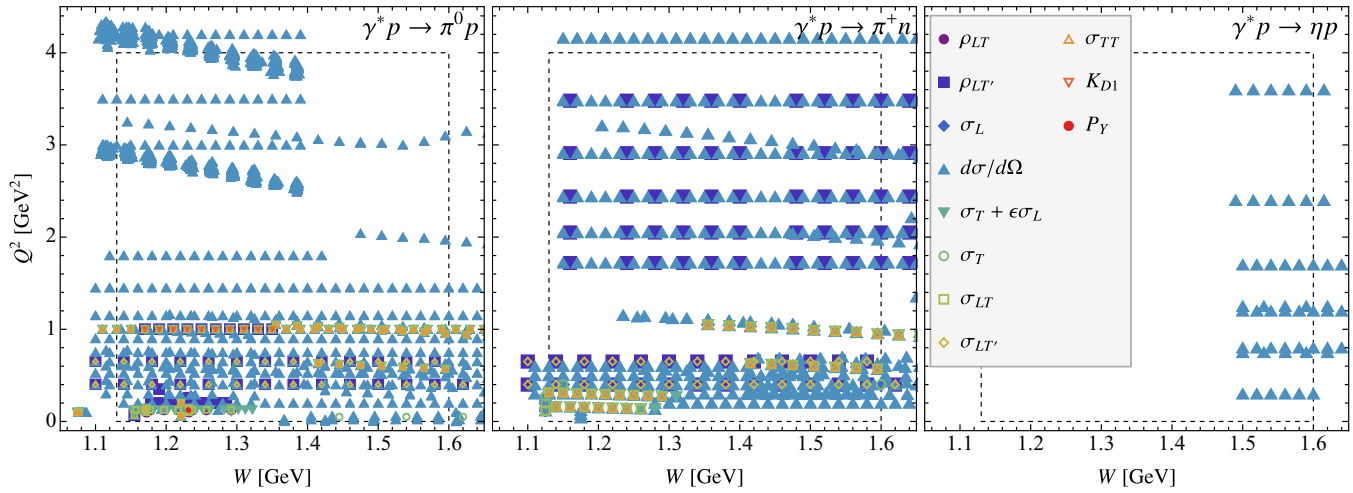


FIG. 3. Experimental data [121–169] used in the present analysis (aggregated values of $\theta$, $\phi$, $\epsilon$). The white dashed rectangles represent the considered fitting window ($0 < Q^2/\text{GeV}^2 < 4$ and $1.13 < W/\text{GeV} < 1.6$).

The data of Ref. [167] were taken for $Q^2$ values of 2.4 and 3.6 GeV$^2$, and for c.m. energies between approximately 1.5 and 1.6 GeV. Cross sections show, within uncertainties, a flat angular distribution, independent of the angle $\phi$. Based on this and a relativistic quark model expectation [171] that longitudinal contributions should be small, a Breit-Wigner-plus-background fit was done to extract the $N(1535)$ contribution. The authors of Ref. [171] concluded that the background was consistent with zero and terms beyond an $S$-wave approximation amounted to less than 7%. The size of longitudinal contributions had also been explored experimentally [172,173] by varying $\epsilon$ in order to extract the ratio of longitudinal and transverse cross sections. This ratio for $Q^2$ values between 0.4 and 1.0 GeV$^2$, and c.m. energies corresponding to the $N(1535)$, was found to be about 20% with 100% uncertainties. Cross sections up to a c.m. energy of 1.9 GeV, for $Q^2$ between 0.15 to 1.5 GeV$^2$, were measured in Ref [169]. Here, the cross section was fitted to an expansion in multipoles up to $J = 3/2$. Unlike Ref. [167], evidence for significant interference between $S$- and $P$-wave contributions was found with cross sections displaying $\theta$ dependence also at a c.m. energy corresponding to the $N(1535)$.

Data from Ref. [168] have the benefit of a wide kinematic range, with c.m. energies between 1.5 and 2.3 GeV, and $Q^2$ values from 0.13 to 3.3 GeV$^2$. Cross sections were expanded in terms of Legendre polynomials. Here too, the angular behavior was concluded to be mainly due to interference between $S$- and $P$-wave contributions, though they could not distinguish between the $N(1710)$ and $N(1720)$ as a source. Fits to this data set tended to show more $\phi$ dependence in the cross section near the $N(1535)$ than was given in the etaMAID result—though these data were not included in the etaMAID solution.

Data from Ref. [174] cover the c.m. energy range from threshold to 1.8 GeV for $Q^2$ values of 5.7 and 7.0 GeV$^2$. Angular behavior is again attributed to $S$- and $P$-wave interference. There is evidence that this interference may change sign in going from lower to higher values of $Q^2$. EtaMAID appears to give a reasonable qualitative description of the data even at these high $Q^2$ values, even though these data were not included in the fit.

TABLE I. Data used in the fit, separated by observable type and final state.

| Type | $N_{\text{data}}^{\pi^0 p}$ | $N_{\text{data}}^{\pi^+ n}$ | $N_{\text{data}}^{\eta p}$ |
|---|---|---|---|
| $\rho_{LT}$ | 45 [121,122] | | |
| $\rho_{LT'}$ | 2644 [123–127] | 4354 [154,155] | |
| $\sigma_L$ | | 2 [156] | |
| $d\sigma/d\Omega$ | 39942 [124,125,128–148] | 32813 [132,148,155,157–166] | 1874 [167–169] |
| $\sigma_T + \epsilon\sigma_L$ | 318 [121,124,128,142,143,149–151] | 144 [158,163] | |
| $\sigma_T$ | 10 [146] | 2 [156] | |
| $\sigma_{LT}$ | 312 [121,124,128,142,143,149–151] | 106 [158,163] | |
| $\sigma_{LT'}$ | 198 [123,142,149,150] | 192 [123] | |
| $\sigma_{TT}$ | 266 [128,142,143,150,151] | 91 [158,163] | |
| $K_{D1}$ | 1527 [125] | | |
| $P_Y$ | | 2 [152,153] | |

TABLE II. Fit results of the coupled-channels JBW analysis with respect to $\pi N$ and $\eta N$ data. The second column shows results of a fit using standard (4.4) ('reg') and weighted (4.5) ('wt') $\chi^2$ functions, respectively, whereas the last three columns separate out contributions for individual final-state channels (per datum).

| | $\chi^2$/dof | $\chi^2_{\pi^0 p/\text{data}}$ | $\chi^2_{\pi^+ n/\text{data}}$ | $\chi^2_{\eta p/\text{data}}$ |
|---|---|---|---|---|
| $\mathfrak{F}_1^{\text{reg}}$ | 1.66 | 1.68 | 1.61 | 1.77 |
| $\mathfrak{F}_2^{\text{reg}}$ | 1.73 | 1.71 | 1.71 | 2.29 |
| $\mathfrak{F}_3^{\text{reg}}$ | 1.69 | 1.69 | 1.66 | 1.89 |
| $\mathfrak{F}_4^{\text{reg}}$ | 1.69 | 1.7 | 1.64 | 2.05 |
| $\mathfrak{F}_1^{\text{wt}}$ | 1.54 | 1.74 | 1.63 | 1.25 |
| $\mathfrak{F}_2^{\text{wt}}$ | 1.63 | 1.82 | 1.79 | 1.27 |
| $\mathfrak{F}_3^{\text{wt}}$ | 1.58 | 1.74 | 1.73 | 1.27 |
| $\mathfrak{F}_4^{\text{wt}}$ | 1.58 | 1.79 | 1.6 | 1.33 |

## IV. DATA AND FITS

By design, the introduced framework is capable of addressing the electroproduction multipoles and observables simultaneously in all considered channels $\{\pi N, \eta N, K\Lambda, K\Sigma, \pi\Delta, \rho N\}$. Experimentally, the most extensively explored final-state channels are $\pi N$, $\eta N$, and $K\Lambda$. Therefore, and also extending upon the already available single channel JBW analysis of Ref. [45], we first restrict the data base to pion and eta final states within the same kinematical range, i.e., $0 < Q^2/\text{GeV}^2 < 4$ and $1.13 < W/\text{GeV} < 1.6$. However, we emphasize that all channels as indicated below Eq. (2.3) in all spin configurations are considered in the intermediate states. The data coverage in this kinematical window is summarized in Fig. 3.

The new $\eta N$ data set consists entirely of differential cross sections, given by

$$\frac{d\sigma}{d\Omega'_e dE_f d\Omega} = \left(\frac{\alpha}{2\pi^2}\frac{E'_e}{E_e}\frac{q_L}{Q^2}\frac{1}{1-\epsilon}\right)\frac{d\sigma^v}{d\Omega}, \tag{4.1}$$

where the solid angle $\Omega$ refers to the angles of the final meson-baryon system $(\theta, \phi)$ and $\Omega'_e$ refers to the final electron at energy $E'_e$. The energy of the initial electron is denoted by $E_e$. The differential cross section $d\sigma^v/d\Omega$ for the virtual photon subprocess is commonly further decomposed as

$$\frac{d\sigma^v}{d\Omega} = \sigma_T + \epsilon\sigma_L + \sqrt{2\epsilon(1+\epsilon)}\sigma_{LT}\cos\phi + \epsilon\sigma_{TT}\cos 2\phi + h\sqrt{2\epsilon(1-\epsilon)}\sigma_{LT'}\sin\phi. \tag{4.2}$$

In contrast, in both $\pi N$ channels also polarization data have been measured which are connected to the multipoles as described explicitly in Ref. [45]. As discussed there, when both differential cross section data and structure functions ($\sigma_T$, $\sigma_L$, $\sigma_{TT}$, $\sigma_{LT}$, and $\sigma_{LT'}$) were available from the same experiment at the same kinematics, double counting was avoided, with preference given to the differential cross section data. This is statistically more sound, as correlations between separated contributions to the differential cross section data are typically not quoted. The combined pion and $\eta$ electroproduction datasets are summarized in Table I.

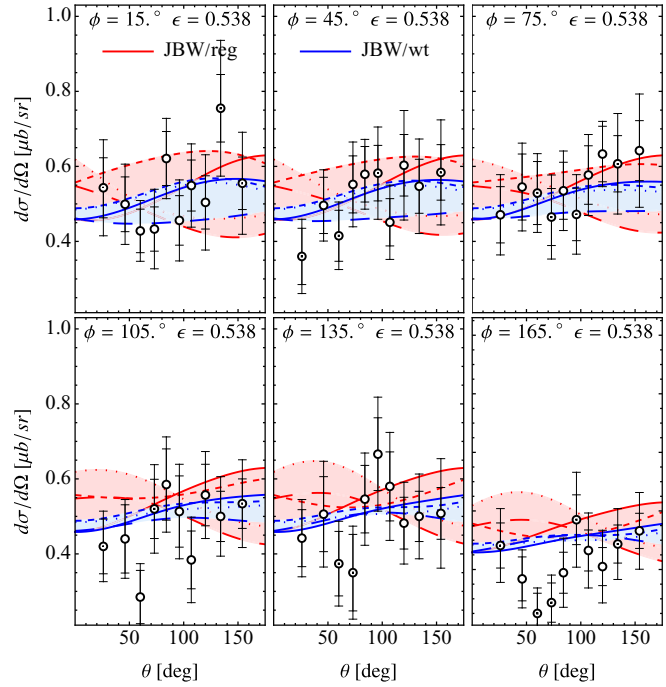


FIG. 4. Selected subset of $\eta N$ data for $W = 1.5$ GeV, $Q^2 = 1.2$ GeV$^2$ from Ref. [168]. The four red and blue lines, respectively, correspond to the "reg" and "wt" solutions of Table II.

To study constraints of the experimental data on the present coupled-channels formalism, we employ the following fit strategies. First, starting with the fit results of the pion-electroproduction analysis [45], including $S$, $P$, and $D$ waves, while setting $N = 2$ in Eq. (2.6), we allow for 40 new parameters,

$$\begin{aligned} &\beta^0_{\eta N},\ \beta^1_{\eta N},\ \beta^2_{\eta N} && \text{for } E_{\ell\pm}, L_{\ell\pm}, M_{\ell\pm}, \text{ and } \ell \leqslant 2, \\ &\zeta^{NP}_{\eta N} && \text{for } L_{1-}, \end{aligned} \tag{4.3}$$

in addition to the 209 previously [45] available parameters. Specifically, for all intermediate channels we chose again $\zeta^{NP}_{\mu\neq\eta N} \equiv \zeta^{NP}_{\pi N}$ and $\beta^{i\in\{0,1,2\}}_{\mu\notin\{\pi N,\eta N\}} = 0$. The choice of $N = 2$ leads to to good fits without signs of overfitting.

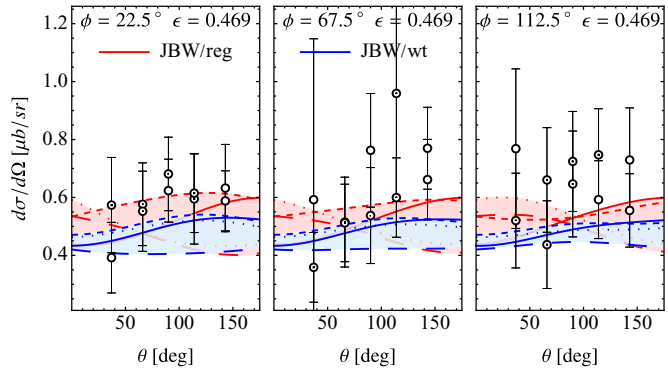


FIG. 5. Selected subset of $\eta N$ data for $W = 1.5$ GeV, $Q^2 = 1.25$ GeV$^2$ from Ref. [169,181]. The four red and blue lines, respectively, correspond to the "reg" and "wt" solutions of Table II.

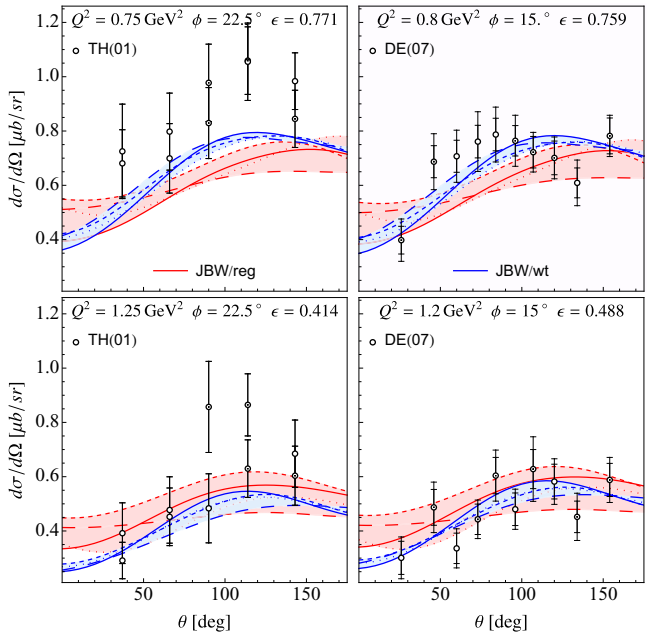


FIG. 6. Selected subset of $\eta N$ data for $W = 1.56$ GeV from Refs. TH(01) [169,181] and DE(07) [168] for similar kinematics. Result of the JBW coupled-channels fits are shown by red and blue lines corresponding to the eight best fit solutions.

Second, starting from any of the four best fit results[1] of Ref. [45] and holding all but the new parameters fixed, we minimize a regular $\chi^2$ function

$$\chi^2_{\rm reg} = \sum_{i=1}^{N_{\rm all}} \left( \frac{\mathcal{O}_i^{\rm exp} - \mathcal{O}_i}{\Delta_i^{\rm stat} + \Delta_i^{\rm syst}} \right)^2 , \tag{4.4}$$

with respect to the data in $\pi^0 p, \pi^+ n, \eta p$ channels simultaneously. The starting values for the 40 new parameters are chosen as $\zeta_{\eta N}^{NP} \equiv \zeta_{\pi N}^{NP}$ and $\beta_{\eta N}^{i\in\{0,1,2\}} = 0$. The data, as taken from SAID, contain also systematic uncertainties $\Delta^{\rm syst}$ that are separately quoted in the database [175]. In this study we choose to add the systematic and statistical error linearly. Adding them in quadrature is also possible but, although they are commonly used, both methods lack the inclusion of correlations of systematic errors. More refined methods (data "floating") have been applied in SAID and JuBo analyses in the past [3,47], and we plan to upgrade the current analysis along these lines. In particular, systematic data shifts can be taken into account by "nuisance parameters" that penalize shifts according to an assumed probability of the systematic error [176]; see also Ref. [177].

We note that the database sizes are vastly different in these channels. Thus, this simple choice of the $\chi^2$ function might marginalize the influence of the smaller $\eta N$ dataset. To test this hypothesis, we additionally perform a minimization with respect to a commonly used weighting scheme (for a typical application see, e.g., [178]),

$$\chi^2_{\rm wt} = \sum_{j\in\{\pi^0 p,\pi^+ n,\eta p\}} \frac{N_{\rm all}}{3N_j} \sum_{i=1}^{N_j} \left( \frac{\mathcal{O}_{ji}^{\rm exp} - \mathcal{O}_{ji}}{\Delta_{ji}^{\rm stat} + \Delta_{ji}^{\rm syst}} \right)^2 . \tag{4.5}$$

Third, after the minimization routine (utilizing the MINUIT library [179]) has converged, all $209 + 40 = 249$ parameters are relaxed and the minimization is repeated leading to the eight different solutions $\{\mathfrak{F}_1^{\rm reg}, \ldots, \mathfrak{F}_4^{\rm reg}, \mathfrak{F}_1^{\rm wt}, \ldots, \mathfrak{F}_4^{\rm wt}\}$, discussed in the next section.

## V. RESULTS

Each of the followed fit strategies led to a successful description of both considered channels. The fit results are collected in Table II including contributions separated out for each of the considered final-state channels ($\pi^0 p$, $\pi^+ n$, $\eta p$). As expected, fit results relying on the weighted version of the $\chi^2$ function (4.5) led to a much better description of the $\eta p$ data, which are much sparser than the $\pi N$ data. When comparing the individual contributions to those of the previous JBW single-channel study [45] we note that the description of both $\pi N$ channels is similar in the present coupled-channels analysis. The same holds true for the contributions to subsets of data separated with respect to individual observable types. For more details on the $\pi N$ channels, see Ref. [45] as well as the interactive JBW homepage [180].

Taking a closer look on the fit results we find a relatively weak $\phi$ dependence in the data and corresponding fits; see Figs. 4 and 5. In the latter figure, there are two data points from Ref. [181] for each angle $\theta$ at a fixed value of $\phi$. These were obtained from measurements at azimuthal angles $\phi$ and $(360^\circ - \phi)$, respectively. The cross sections were averaged in Ref. [169], but both values are retained in our database. In Fig. 6 we compare fits and data at nearby kinematic points for which the fit curves are nearly identical. This gives a visual comparison of the data consistency.

As for underlying multipoles, we found that in most cases longitudinal multipoles are subdominant to electric and magnetic ones. An overview of all considered multipoles is shown in Fig. 7 for the c.m. energy fixed to 1535 MeV. There, in most cases and within the systematic uncertainties of our approach, quantified by the spread of predictions from fits $\{\mathfrak{F}_1^{\rm reg}, \ldots, \mathfrak{F}_4^{\rm reg}, \mathfrak{F}_1^{\rm wt}, \ldots, \mathfrak{F}_4^{\rm wt}\}$, we observe an agreement with the MAID2007 ($\pi N$) and etaMAID ($\eta N$) multipole predictions.[2] The isospin $I = 1/2$ $\pi N$ multipoles are shown in the same figure with the pertinent comparison to the MAID2007 solution for convenience.

Fixing the virtuality $Q^2$ to some values of interest the multipoles are shown in Figs. 9 and 10. There, we observe that the dominant $E_{0+}$ multipole agrees well with that of the

[1] These solutions were obtained following different fit strategies in order to obtain a representation of the systematic uncertainty. The two solutions of Ref. [45], with extended $Q^2$ ranges of up to 8 GeV$^2$, are not used in this work.

[2] A more quantitative statement is impossible due to missing uncertainty estimations for the etaMAID parametrizations.

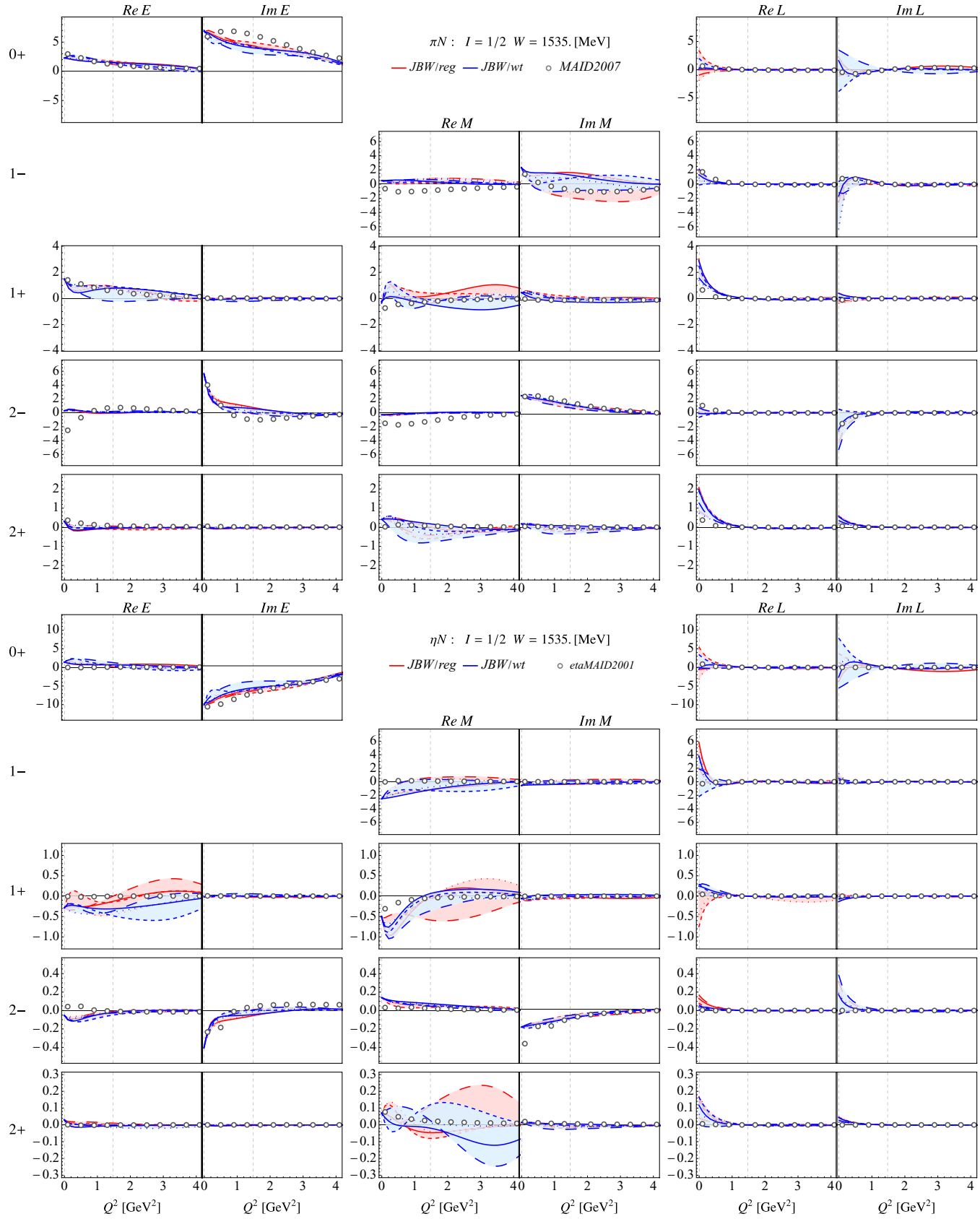


FIG. 7. JBW coupled-channels results. Multipoles (in mfm, referring to milli-femtometer [$10^{-18}$ m]) in the $\pi N$ and $\eta N$ $I = 1/2$ channel at $W = 1535$ MeV in comparison to the result of the MAID2007 [35] and etaMAID2001 [33] analyses, respectively. The latter results are extracted from the MAID homepage and multiplied by $-1/\sqrt{3}$, adjusting for a phase- and isospin factor. The leftmost column shows the total angular momentum. Fits correspond to the results of Tabe II with the same line shape coding as in Ref [45].

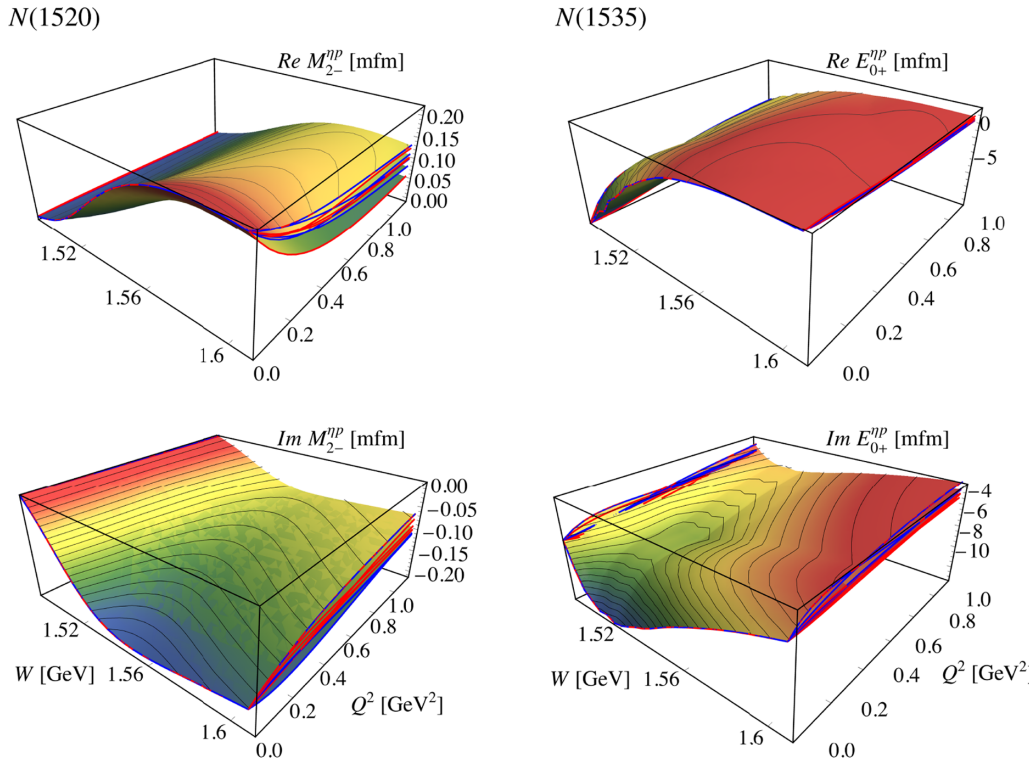


FIG. 8. Predictions of multipoles corresponding to the quantum numbers of $N(1520)$ (left) and $N(1535)$ (right). Different surfaces correspond to the best fit solutions obtained minimizing the regular (red boundary lines) and weighted (blue boundary lines) version of the $\chi^2$ function.

etaMAID parametrization when correcting for the phase convention $(-1)$ and isospin factor $(1/\sqrt{3})$. To be clear, we show our multipoles in the isospin basis, which make them smaller by a factor of $1/\sqrt{3}$ compared to the etaMAID multipoles which are quoted in the particle basis. As the results show, longitudinal multipoles seem indeed very small compared to the electric and magnetic ones. Interestingly, the $M_{2-}$ multipole seems to have a similar trend as that of the MAID solution, while the corresponding uncertainties seem to change with different $Q^2$ values. This can be attributed to the gaps in $\eta p$ data at some fixed $Q^2$ kinematics; see the next section.

Finally, we demonstrate in Fig. 8 the full $Q^2$ vs $W$ dependence of the $E_{0+}$ and $M_{2-}$ multipoles, corresponding to quantum numbers of the $N(1535)1/2^-$ and $N(1520)3/2^-$. We observe that the systematic uncertainties discussed above are well under control. In particular, all fit solutions show a nontrivial $Q^2$ dependence. This supports our expectation that the helicity couplings will carry new physical information, when full $(W, Q^2)$ information is extracted, being part of our future plans.

## VI. DISCUSSION AND CONCLUSION

We have generalized our recent analysis of pion electroproduction [45] to include $\eta$ electroproduction data. This allowed a coupled-channels fit up to $W = 1.6$ GeV for $Q^2 < 4$ GeV$^2$. For both reactions, partial waves up to $\ell = 2$ were included. Given that the pion and $\eta$ electroproduction databases are very different in size, we compared $\chi^2$ minimization without and with weighting factors to increase the influence of the smaller $\eta$ electroproduction dataset.

As in Ref. [26], using different fit strategies, we found several solutions with nearly equivalent $\chi^2$/data values. The fits achieved $\chi^2$/data values near 1.7, similar to our previous fits to pion data alone. The fit to pion data and the resulting multipoles showed little change from the single-channel case. This result held in both weighted and unweighted fits.

Also, as in our pion electroproduction fits, the spread of results for multipoles provided a measure of systematic errors. As expected, the $E_{0+}$ multipole was reliably determined with a $Q^2$ dependence similar to that exhibited in etaMAID (once a phase ambiguity was accounted for).

The evidence for contributions from higher partial waves depends on the experiment. As mentioned, the data of Ref. [167] are compatible with a Breit-Wigner contribution from the $N(1535)$, without any need for a background term, higher partial waves, or longitudinal multipoles, for a fit covering the energy range considered in the present analysis. The later experiment of Ref. [168], however, displays a clear forward-backward asymmetry (a sign of $P$-wave interference) and some evidence for $D$-wave interference producing a convex shape.

In our multipole solutions, there is evidence for sizable $P$-wave contributions, but the spread implies the $P$-wave multipoles are not well determined. This is expected since the corresponding candidate states $N(1710)1/2^+$ and $N(1720)3/2^+$ are beyond the upper energy limit. Interestingly, the $M_{2-}$ multipoles are quite consistent, and appear to give a consistent

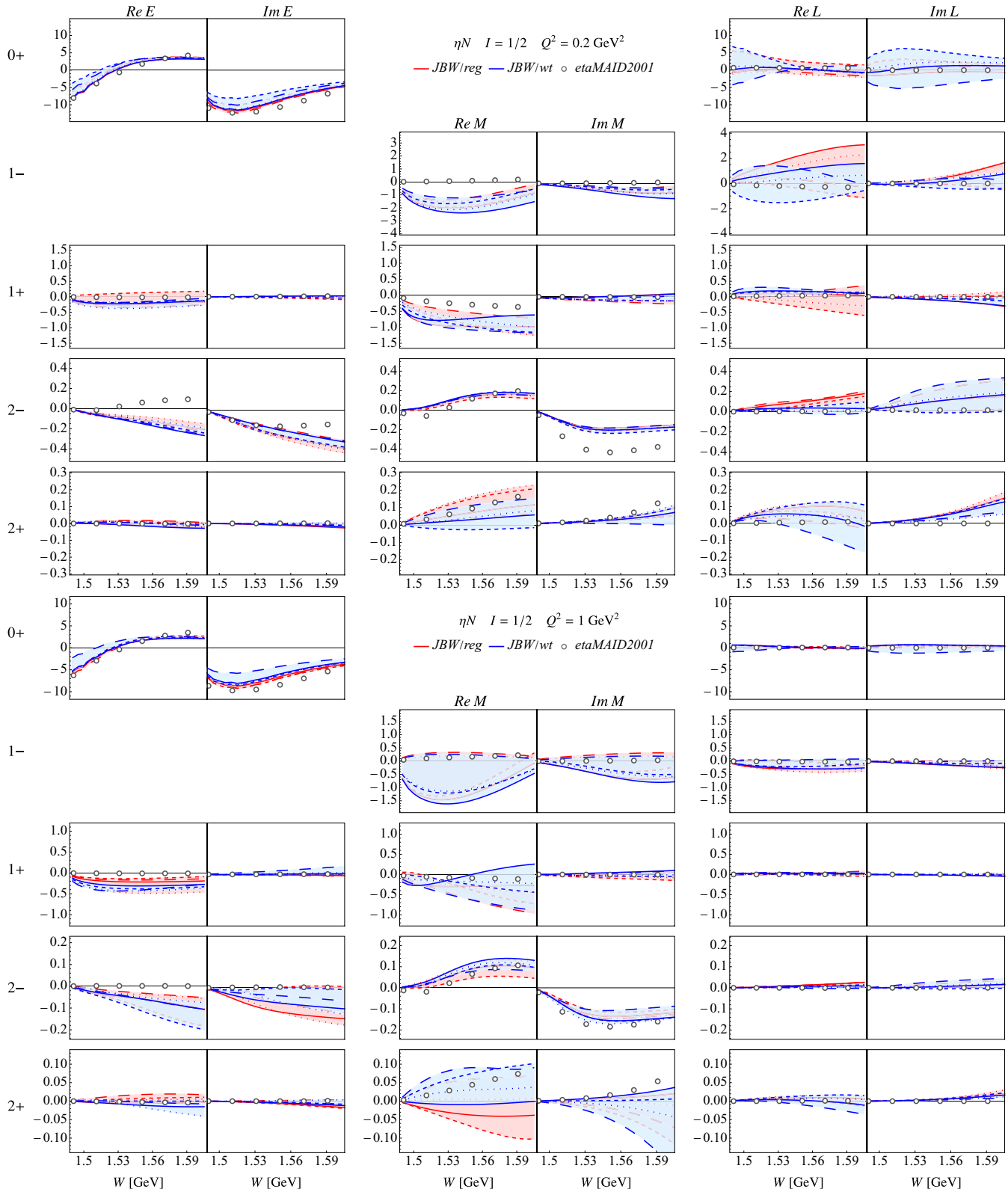


FIG. 9. $\eta$ electroproduction multipoles for lower fixed values of $Q^2$. Notation as given in Fig. 7.

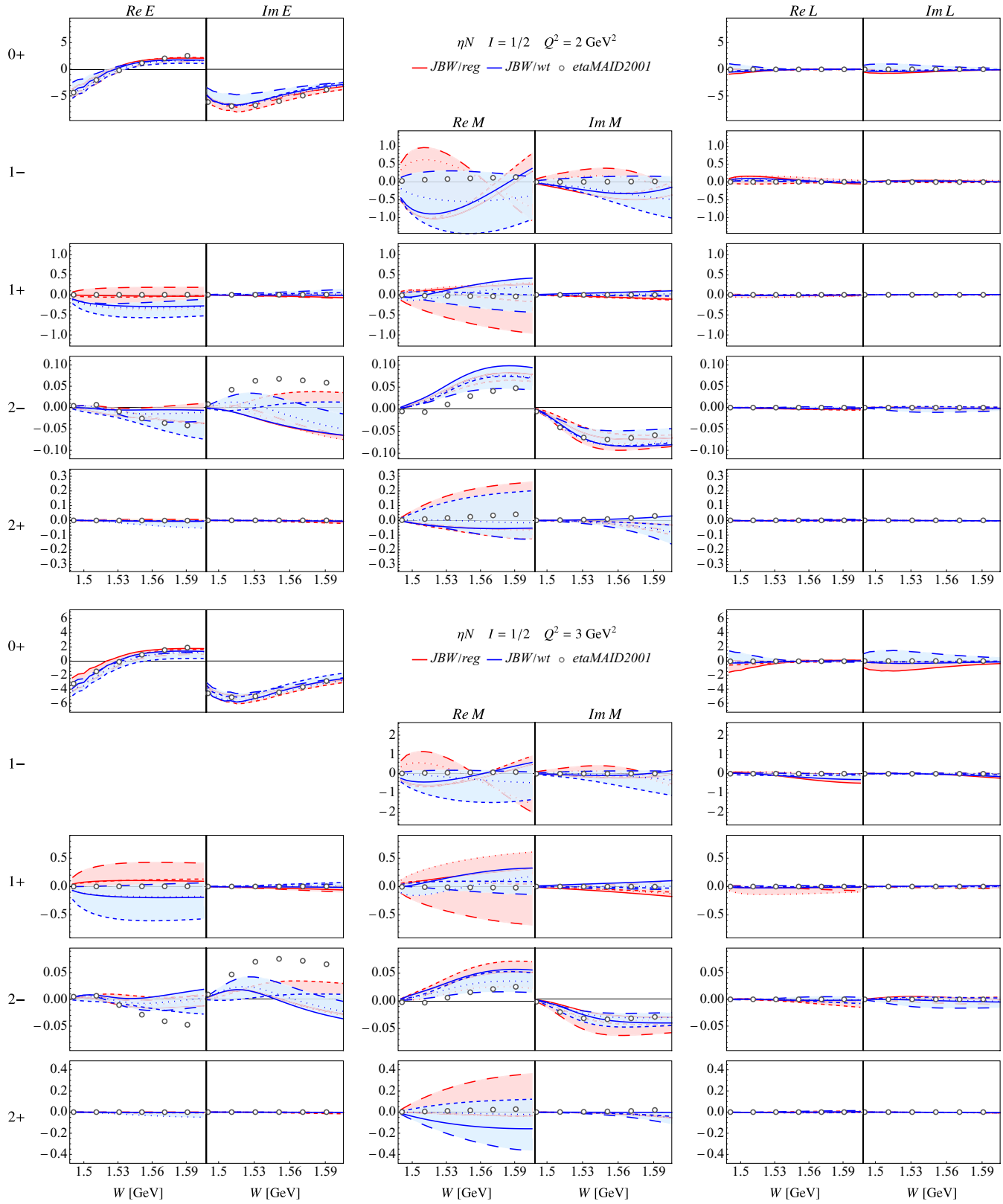


FIG. 10. $\eta$ electroproduction multipoles for higher fixed values of $Q^2$. Notation as given in Fig. 7.

value for this multipole, which also agrees with the etaMAID values away from the $Q^2 = 0$ photon point and the upper $Q^2$ limit of our fits.

We can understand the consistency of multipole determinations in Figs. 9 and 10, plotting multipoles versus center-of-mass energy for fixed $Q^2$ (0.2, 1, 2, and 3 GeV$^2$), based on the data fitted and the constraint at $Q^2 = 0$. The lowest-$Q^2$ plot displays multipoles for a $Q^2$ value below the lower limit (0.3 GeV$^2$) of fitted data and is close to the photoproduction point, where it was shown that the etaMAID and JüBo fits can be quite different. The behavior at $Q^2 = 3$ GeV$^2$ is supported by data from Ref. [167] (2.4 and 3.6 GeV$^2$) which can be fitted with only a Breit-Wigner contribution to $E_{0+}$ and shows no evidence for $P$ and $D$ waves.

The plots for intermediate $Q^2$ are supported by data from Refs. [168,169], of which Ref. [168] is more precise. These plots show the most consistency for multipoles that can be determined over this narrow energy range. Note also that longitudinal multipoles are small (consistently among all our solutions) whereas this feature was built in in some earlier fits [167].

In summary, this first coupled-channels fit to both pion and $\eta$ electroproduction data supports an expanded study. As a first step, the number of included partial-waves and the energy limits will be increased. Once completed, we will attempt an expansion to kaon electroproduction [8,182–187], in the near-threshold region. We will also be in a position to explore resonance behavior at the pole as a function of $Q^2$ using tools developed to study the JüBo photoproduction amplitudes.

## ACKNOWLEDGMENTS

This work is supported by the U.S. Department of Energy, DOE Office of Science, Office of Nuclear Physics Awards No. DE-SC0016582 and No. DE-SC0016583 and Contract No. DE-AC05-06OR23177. This material is based upon work supported by the National Science Foundation under Grant No. PHY 2012289. It is also supported by the NSFC and the Deutsche Forschungsgemeinschaft (DFG, German Research Foundation) through the funds provided to the Sino-German Collaborative Research Center TRR110 Symmetries and the Emergence of Structure in QCD (NSFC Grant No. 12070131001, DFG Project-ID 196253076-TRR 110), by the Chinese Academy of Sciences (CAS) through a President's International Fellowship Initiative (PIFI) (Grant No. 2018DM0034), by the VolkswagenStiftung (Grant No. 93562), and by the EU Horizon 2020 research and innovation program, STRONG-2020 project under Grant Agreement No. 824093. The multipole calculation and parameter optimization are performed on the Colonial One computer cluster [188]. The authors gratefully acknowledge the computing time granted through JARA on the supercomputer JURECA [189] at Forschungszentrum Jülich that was used to produce the input at the photon point.

[1] G. Höhler, in *Methods and Results of Phenomenological Analyses (Methoden und Ergebnisse phänomenologischer Analysen)*, edited by H. Schopper, Landolt-Boernstein, Group I Elementary Particles, Nuclei and Atoms, Vol. 9b2 (Springer, Berlin, 1983).

[2] R. E. Cutkosky, R. E. Hendrick, J. W. Alcock, Y. A. Chao, R. G. Lipes, J. C. Sandusky, and R. L. Kelly, Pion-nucleon partial wave analysis, Phys. Rev. D **20**, 2804 (1979).

[3] R. A. Arndt, W. J. Briscoe, I. I. Strakovsky, and R. L. Workman, Extended partial-wave analysis of $\pi N$ scattering data, Phys. Rev. C **74**, 045205 (2006).

[4] R. A. Arndt, W. J. Briscoe, M. W. Paris, I. I. Strakovsky, and R. L. Workman, Baryon resonance analysis from SAID, Chin. Phys. C **33**, 1063 (2009).

[5] M. Shrestha and D. M. Manley, Multichannel parametrization of $\pi N$ scattering amplitudes and extraction of resonance parameters, Phys. Rev. C **86**, 055203 (2012).

[6] D. G. Ireland, E. Pasyuk, and I. Strakovsky, Photoproduction reactions and non-strange baryon spectroscopy, Prog. Part. Nucl. Phys. **111**, 103752 (2020).

[7] I. G. Aznauryan *et al.* (CLAS Collaboration), Electroexcitation of nucleon resonances from CLAS data on single pion electroproduction, Phys. Rev. C **80**, 055203 (2009).

[8] P. Achenbach *et al.* (A1 Collaboration), Beam helicity asymmetries in $K^+\Lambda$ electroproduction off the proton at low $Q^2$, Eur. Phys. J. A **53**, 198 (2017).

[9] D. S. Carman, K. Joo, and V. I. Mokeev, Strong QCD insights from excited nucleon structure studies with CLAS and CLAS12, Few Body Syst. **61**, 29 (2020).

[10] R. Beck and U. Thoma, Spectroscopy of baryon resonances, EPJ Web Conf. **134**, 02001 (2017).

[11] S. H. Shiu *et al.* (LEPS Collaboration), Photoproduction of $\Lambda$ and $\Sigma^0$ hyperons off protons with linearly polarized photons at $E_\gamma = 1.5$–$3.0$ GeV, Phys. Rev. C **97**, 015208 (2018).

[12] C. S. Akondi *et al.* (A2 Collaboration), Experimental study of the $\gamma p \to K^0\Sigma^+$, $\gamma n \to K^0\Lambda$, and $\gamma n \to K^0\Sigma^0$ reactions at the Mainz Microtron, Eur. Phys. J. A **55**, 202 (2019).

[13] D. H. Ho *et al.* (CLAS Collaboration), Beam-target helicity asymmetry $E$ in $K^0\Lambda$ and $K^0\Sigma^0$ photoproduction on the neutron, Phys. Rev. C **98**, 045205 (2018).

[14] H. Ohnishi, F. Sakuma, and T. Takahashi, Hadron physics at J-PARC, Prog. Part. Nucl. Phys. **113**, 103773 (2020).

[15] S. Alef *et al.* (BGO-OD Collaboration), The BGOOD experimental setup at ELSA, Eur. Phys. J. A **56**, 104 (2020).

[16] N. Zachariou *et al.* (CLAS Collaboration), Double polarisation observable $\mathbb{G}$ for single pion photoproduction from the proton, Phys. Lett. B **817**, 136304 (2021).

[17] U. Shrestha *et al.* (CLAS Collaboration), Differential cross sections for $\Lambda(1520)$ using photoproduction at CLAS, Phys. Rev. C **103**, 025206 (2021).

[18] S.H. Shiu, H. Kohri, W.C. Chang, D.S. Ahn, J.K. Ahn, J.Y. Chen, S. Date, H. Ejiri, H. Fujimura, M. Fujiwara, S. Fukui, W. Gohn, K. Hicks, T. Hotta, S.H. Hwang, K. Imai, T. Ishikawa, K. Joo, Y. Kato, Y. Kon *et al.*, (CLAS Collaboration), Exclusive $\pi^0 p$ electroproduction off protons in the resonance region at photon virtualities 0.4 GeV$^2 \leqslant Q^2 \leqslant 1$ GeV$^2$, Phys. Rev. C **101**, 015208 (2020).

[19] V. Bernard, N. Kaiser, and Ulf G. Meißner, On the low-energy theorems for threshold pion electroproduction, Phys. Lett. B **282**, 448 (1992).

[20] V. Bernard, N. Kaiser, T. S. H. Lee, and Ulf-G. Meißner, Chiral Symmetry and Threshold $\pi^0$ Electroproduction, Phys. Rev. Lett. **70**, 387 (1993).

[21] V. Bernard, N. Kaiser, T. S. H. Lee, and Ulf-G. Meißner, Threshold pion electroproduction in chiral perturbation theory, Phys. Rep. **246**, 315 (1994).

[22] V. Bernard, N. Kaiser, and Ulf-G. Meißner, Threshold neutral pion electroproduction in heavy baryon chiral perturbation theory, Nucl. Phys. A **607**, 379 (1996); **633**, 695(E) (1998).

[23] M. Hilt, B. C. Lehnhart, S. Scherer, and L. Tiator, Pion photo- and electroproduction in relativistic baryon chiral perturbation theory and the chiral MAID interface, Phys. Rev. C **88**, 055207 (2013).

[24] M. Mai, Review of the $\Lambda(1405)$: A curious case of a strangeness resonance, Eur. Phys. J. ST **230**, 1593 (2021).

[25] D. Ruić, M. Mai, and Ulf-G. Meißner, $\eta$-photoproduction in a gauge-invariant chiral unitary framework, Phys. Lett. B **704**, 659 (2011).

[26] M. Mai, P. C. Bruns, and Ulf-G. Meißner, Pion photoproduction off the proton in a gauge-invariant chiral unitary framework, Phys. Rev. D **86**, 094033 (2012).

[27] P. C. Bruns, A formalism for the study of $K^+\pi$ $\Sigma$ photoproduction in the $\Lambda^*(1405)$ region, arXiv:2012.11298.

[28] M. Döring and K. Nakayama, On the cross section ratio $\sigma_n/\sigma_p$ in $\eta$ photoproduction, Phys. Lett. B **683**, 145 (2010).

[29] M. Döring and K. Nakayama, The phase and pole structure of the $N^*(1535)$ in $\pi N \to \pi N$ and $\gamma N \to \pi N$, Eur. Phys. J. A **43**, 83 (2010).

[30] B. Borasoy, P. C. Bruns, Ulf-G. Meißner, and R. Nissler, A gauge invariant chiral unitary framework for kaon photo- and electroproduction on the proton, Eur. Phys. J. A **34**, 161 (2007).

[31] Ulf-G. Meißner and J. A. Oller, Chiral unitary meson baryon dynamics in the presence of resonances: Elastic pion nucleon scattering, Nucl. Phys. A **673**, 311 (2000).

[32] H. Haberzettl, Gauge invariance of meson photo- and electroproduction currents revisited, Phys. Rev. D **104**, 056001 (2021).

[33] W.-T. Chiang, S.-N. Yang, L. Tiator, and D. Drechsel, An isobar model for eta photoproduction and electroproduction on the nucleon, Nucl. Phys. A **700**, 429 (2002).

[34] I. G. Aznauryan, Multipole amplitudes of pion photoproduction on nucleons up to 2 GeV within dispersion relations and unitary isobar model, Phys. Rev. C **67**, 015209 (2003).

[35] D. Drechsel, S. S. Kamalov, and L. Tiator, Unitary Isobar Model - MAID2007, Eur. Phys. J. A **34**, 69 (2007).

[36] L. Tiator, M. Gorchtein, V. L. Kashevarov, K. Nikonov, M. Ostrick, M. Hadžimehmedović, R. Omerović, H. Osmanović, J. Stahov, and A. Švarc, $\eta$ and $\eta'$ photoproduction on the nucleon with the isobar model EtaMAID2018, Eur. Phys. J. A **54**, 210 (2018).

[37] O. Hanstein, D. Drechsel, and L. Tiator, Multipole analysis of pion photoproduction based on fixed $t$ dispersion relations and unitarity, Nucl. Phys. A **632**, 561 (1998).

[38] R. L. Workman, M. W. Paris, W. J. Briscoe, and I. I. Strakovsky, Unified Chew-Mandelstam SAID analysis of pion photoproduction data, Phys. Rev. C **86**, 015202 (2012).

[39] W. J. Briscoe, M. Döring, H. Haberzettl, D. M. Manley, M. Naruki, I. I. Strakovsky, and E. S. Swanson, Physics opportunities with meson beams, Eur. Phys. J. A **51**, 129 (2015).

[40] V. Shklyar, H. Lenske, and U. Mosel, $\eta$ photoproduction in the resonance energy region, Phys. Lett. B **650**, 172 (2007).

[41] A. V. Anisovich, R. Beck, E. Klempt, V. A. Nikonov, A. V. Sarantsev, and U. Thoma, Properties of baryon resonances from a multichannel partial wave analysis, Eur. Phys. J. A **48**, 15 (2012).

[42] H. Kamano, S. X. Nakamura, T. S. H. Lee, and T. Sato, Nucleon resonances within a dynamical coupled-channels model of $\pi N$ and $\gamma N$ reactions, Phys. Rev. C **88**, 035209 (2013).

[43] D. Rönchen, M. Döring, H. Haberzettl, J. Haidenbauer, U. G. Meißner, and K. Nakayama, $\eta$ photoproduction in a combined analysis of pion- and photon-induced reactions, Eur. Phys. J. A **51**, 70 (2015).

[44] J. Nys, V. Mathieu, C. Fernández-Ramírez, A. N. Hiller Blin, A. Jackura, M. Mikhasenko, A. Pilloni, A. P. Szczepaniak, G. Fox, and J. Ryckebusch (JPAC Collaboration), Finite-energy sum rules in $\eta$ photoproduction off a nucleon, Phys. Rev. D **95**, 034014 (2017).

[45] M. Mai, M. Döring, C. Granados, H. Haberzettl, Ulf-G. Meißner, D. Rönchen, I. Strakovsky, and R. Workman (Jülich-Bonn-Washington Collaboration), Jülich-Bonn-Washington model for pion electroproduction multipoles, Phys. Rev. C **103**, 065204 (2021).

[46] A. Thiel, F. Afzal, and Y. Wunderlich, Light baryon spectroscopy, Prog. Part. Nucl. Phys. **125**, 103949 (2022).

[47] D. Rönchen, M. Döring, and U.-G. Meißner, The impact of $K^+\Lambda$ photoproduction on the resonance spectrum, Eur. Phys. J. A **54**, 110 (2018).

[48] H. Kamano, S. X. Nakamura, T. S. H. Lee, and T. Sato, Isospin decomposition of $\gamma N \to N^*$ transitions within a dynamical coupled-channels model, Phys. Rev. C **94**, 015201 (2016).

[49] D. Rönchen, M. Döring, F. Huang, H. Haberzettl, J. Haidenbauer, C. Hanhart, S. Krewald, U.-G. Meißner, and K. Nakayama, Photocouplings at the pole from pion photoproduction, Eur. Phys. J. A **50**, 101 (2014); **51**, 63(E) (2015).

[50] H. Kamano, S. X. Nakamura, T. S. H. Lee, and T. Sato, Extraction of $P_{11}$ resonances from $\pi N$ data, Phys. Rev. C **81**, 065207 (2010).

[51] L. Tiator, S. S. Kamalov, S. Ceci, G. Y. Chen, D. Drechsel, A. Svarc, and S. N. Yang, Singularity structure of the $\pi N$ scattering amplitude in a meson-exchange model up to energies $W \leqslant 2.0$ GeV, Phys. Rev. C **82**, 055203 (2010).

[52] P. A. Zyla *et al.* (Particle Data Group), Review of particle physics, Prog. Theor. Exp. Phys. **2020**, 083C01 (2020).

[53] V. Crede *et al.* (CBELSA/TAPS Collaboration), Photoproduction of neutral pions off protons, Phys. Rev. C **84**, 055203 (2011).

[54] A. V. Anisovich, V. Burkert, J. Hartmann, E. Klempt, V. A. Nikonov, E. Pasyuk, A. V. Sarantsev, S. Strauch, and U. Thoma, Evidence for $\Delta(2200)7/2^-$ from photoproduction and consequence for chiral-symmetry restoration at high mass, Phys. Lett. B **766**, 357 (2017).

[55] J. Landay, M. Mai, M. Döring, H. Haberzettl, and K. Nakayama, Towards the minimal spectrum of excited baryons, Phys. Rev. D **99**, 016001 (2019).

[56] J. Landay, M. Döring, C. Fernández-Ramírez, B. Hu, and R. Molina, Model selection for pion photoproduction, Phys. Rev. C **95**, 015203 (2017).

[57] D. Drechsel, O. Hanstein, S. S. Kamalov, and L. Tiator, A Unitary isobar model for pion photoproduction and

electroproduction on the proton up to 1 GeV, Nucl. Phys. A **645**, 145 (1999).
[58] R. A. Arndt, I. I. Strakovsky, and R. L. Workman, Analysis of pion electroproduction data, PiN Newslett. **16**, 150 (2002).
[59] L. Tiator, D. Drechsel, S. S. Kamalov, and S. N. Yang, Electromagnetic form-factors of the $\Delta(1232)$ excitation, Eur. Phys. J. A **17**, 357 (2003).
[60] L. Tiator, D. Drechsel, S. Kamalov, M. M. Giannini, E. Santopinto, and A. Vassallo, Electroproduction of nucleon resonances, Eur. Phys. J. A **19**, 55 (2004).
[61] I. G. Aznauryan, V. D. Burkert, H. Egiyan, K. Joo, R. Minehart, and L. C. Smith, Electroexcitation of the $P_{33}(1232)$, $P_{11}(1440)$, $D_{13}(1520)$, and $S_{11}(1535)$ at $Q^2 = 0.4$ and $0.65(\mathrm{GeV}/c)^2$, Phys. Rev. C **71**, 015201 (2005).
[62] I. G. Aznauryan, V. D. Burkert, G. V. Fedotov, B. S. Ishkhanov, and V. I. Mokeev, Electroexcitation of nucleon resonances at $Q^2 = 0.65(\mathrm{GeV}/c)^2$ from a combined analysis of single- and double-pion electroproduction data, Phys. Rev. C **72**, 045201 (2005).
[63] T. Corthals, T. Van Cauteren, P. Van Craeyveld, J. Ryckebusch, and D. G. Ireland, Electroproduction of kaons from the proton in a Regge-plus-resonance approach, Phys. Lett. B **656**, 186 (2007).
[64] I. G. Aznauryan and V. D. Burkert, Electroexcitation of nucleon resonances, Prog. Part. Nucl. Phys. **67**, 1 (2012).
[65] L. Tiator, D. Drechsel, S. S. Kamalov, and M. Vanderhaeghen, Electromagnetic excitation of nucleon resonances, Eur. Phys. J. Spec. Top. **198**, 141 (2011).
[66] I. G. Aznauryan *et al.*, Studies of nucleon resonance structure in exclusive meson electroproduction, Int. J. Mod. Phys. E **22**, 1330015 (2013).
[67] T. Vrancx, J. Ryckebusch, and J. Nys, $K^+\Lambda$ electroproduction above the resonance region, Phys. Rev. C **89**, 065202 (2014).
[68] O. V. Maxwell, Recoil polarization observables in the electroproduction of $K$ mesons and $\Lambda$'s from the proton, Phys. Rev. C **90**, 034605 (2014).
[69] V. I. Mokeev, V. D. Burkert, D. S. Carman, L. Elouadrhiri, G. V. Fedotov, E. N. Golovatch, R. W. Gothe, K. Hicks, B. S. Ishkhanov, E. L. Isupov, and I. Skorodumina, New results from the studies of the $N(1440)1/2^+$, $N(1520)3/2^-$, and $\Delta(1620)1/2^-$ resonances in exclusive $ep \to e'p'\pi^+\pi^-$ electroproduction with the CLAS detector, Phys. Rev. C **93**, 025206 (2016).
[70] S. X. Nakamura, H. Kamano, and T. Sato, Dynamical coupled-channels model for neutrino-induced meson productions in resonance region, Phys. Rev. D **92**, 074024 (2015).
[71] E. L. Isupov *et al.* (CLAS Collaboration), Measurements of $ep \to e'\pi^+\pi^-p'$ Cross Sections with CLAS at 1.40 Gev $< W <$ 2.0 GeV and 2.0 $\mathrm{GeV}^2 < Q^2 <$ 5.0 $\mathrm{GeV}^2$, Phys. Rev. C **96**, 025209 (2017).
[72] L. Tiator, R. L. Workman, Y. Wunderlich, and H. Haberzettl, Amplitude reconstruction from complete electroproduction experiments and truncated partial-wave expansions, Phys. Rev. C **96**, 025210 (2017).
[73] V. D. Burkert, V. I. Mokeev, and B. S. Ishkhanov, The nucleon resonance structure from the $\pi^+\pi^-p$ electroproduction reaction off protons, Moscow Univ. Phys. Bull. **74**, 243 (2019).
[74] A. N. HillerBlin, V. Mokeev, M. Albaladejo, C. Fernandez-Ramirez, V. Mathieu, A. Pilloni, A. Szczepaniak, V. D. Burkert, V. V. Chesnokov, A. A. Golubenko, and M. Vanderhaeghen, Nucleon resonance contributions to unpolarized inclusive electron scattering, Phys. Rev. C **100**, 035201 (2019).
[75] T. Mart, C. Bennhold, and H. Haberzettl, An isobar model for the photoproduction and electroproduction of kaons on the nucleon, PiN Newslett. **16**, 86 (2002).
[76] V. I. Mokeev *et al.*, Evidence for the $N'(1720)3/2^+$ nucleon resonance from combined studies of CLAS $\pi^+\pi^-p$ photo- and electroproduction data, Phys. Lett. B **805**, 135457 (2020).
[77] A. N. Hiller Blin, W. Melnitchouk, V. I. Mokeev, V. D. Burkert, V. V. Chesnokov, A. Pilloni, and A. P. Szczepaniak, Resonant contributions to inclusive nucleon structure functions from exclusive meson electroproduction data, Phys. Rev. C **104**, 025201 (2021).
[78] Y. Wunderlich, P. Kroenert, F. Afzal, and A. Thiel, Moravcsik's theorem on complete sets of polarization observables reexamined, Phys. Rev. C **102**, 034605 (2020).
[79] Y. Wunderlich, New graphical criterion for the selection of complete sets of polarization observables and its application to single-meson photoproduction as well as electroproduction, Phys. Rev. C **104**, 045203 (2021).
[80] N. Isgur and G. Karl, $P$ wave baryons in the quark model, Phys. Rev. D **18**, 4187 (1978).
[81] S. Capstick and N. Isgur, Baryons in a relativized quark model with chromodynamics, AIP Conf. Proc. **132**, 267 (1985).
[82] S. Capstick, Photoproduction and electroproduction of nonstrange baryon resonances in the relativized quark model, Phys. Rev. D **46**, 2864 (1992).
[83] S. Capstick and W. Roberts, Quasi-two-body decays of nonstrange baryons, Phys. Rev. D **49**, 4570 (1994).
[84] M. Ronniger and B. C. Metsch, Effects of a spin-flavour dependent interaction on the baryon mass spectrum, Eur. Phys. J. A **47**, 162 (2011).
[85] G. Ramalho and M. T. Pena, A covariant model for the $\gamma N \to N(1535)$ transition at high momentum transfer, Phys. Rev. D **84**, 033007 (2011).
[86] C. Jayalath, J. L. Goity, E. Gonzalez de Urreta, and N. N. Scoccola, Negative parity baryon decays in the $1/N_c$ expansion, Phys. Rev. D **84**, 074012 (2011).
[87] I. G. Aznauryan and V. D. Burkert, Nucleon electromagnetic form factors and electroexcitation of low lying nucleon resonances in a light-front relativistic quark model, Phys. Rev. C **85**, 055202 (2012).
[88] B. Golli and S. Širca, A chiral quark model for meson electroproduction in the region of $D$-wave resonances, Eur. Phys. J. A **49**, 111 (2013).
[89] I. T. Obukhovsky, A. Faessler, D. K. Fedorov, T. Gutsche, and V. E. Lyubovitskij, Transition form factors and helicity amplitudes for electroexcitation of negative- and positive parity nucleon resonances in a light-front quark model, Phys. Rev. D **100**, 094013 (2019).
[90] G. Ramalho, M. T. Peña, and K. Tsushima, Hyperon electromagnetic timelike elastic form factors at large $q^2$, Phys. Rev. D **101**, 014014 (2020).
[91] G. Ramalho and M. T. Peña, Covariant model for the Dalitz decay of the $N(1535)$ resonance, Phys. Rev. D **101**, 114008 (2020).
[92] C. D. Roberts and A. G. Williams, Dyson-Schwinger equations and their application to hadronic physics, Prog. Part. Nucl. Phys. **33**, 477 (1994).
[93] C. D. Roberts, Hadron properties and Dyson-Schwinger equations, Prog. Part. Nucl. Phys. **61**, 50 (2008).

[94] G. Eichmann, R. Alkofer, A. Krassnigg, and D. Nicmorus, Nucleon Mass From a Covariant Three-quark Faddeev Equation, Phys. Rev. Lett. **104**, 201601 (2010).

[95] D. J. Wilson, I. C. Cloet, L. Chang, and C. D. Roberts, Nucleon and Roper electromagnetic elastic and transition form factors, Phys. Rev. C **85**, 025205 (2012).

[96] C. Chen, L. Chang, C. D. Roberts, S. Wan, and D. J. Wilson, Spectrum of hadrons with strangeness, Few Body Syst. **53**, 293 (2012).

[97] G. Eichmann and C. S. Fischer, Nucleon Compton scattering in the Dyson-Schwinger approach, Phys. Rev. D **87**, 036006 (2013).

[98] S.-S. Xu, C. Chen, I. C. Cloet, C. D. Roberts, J. Segovia, and H.-S. Zong, Contact-interaction Faddeev equation and, *inter alia*, proton tensor charges, Phys. Rev. D **92**, 114034 (2015).

[99] J. Segovia, B. El-Bennich, E. Rojas, I. C. Cloet, C. D. Roberts, S.-S. Xu, and H.-S. Zong, Completing the Picture of the Roper Resonance, Phys. Rev. Lett. **115**, 171801 (2015).

[100] G. Eichmann, H. Sanchis-Alepuz, R. Williams, R. Alkofer, and C. S. Fischer, Baryons as relativistic three-quark bound states, Prog. Part. Nucl. Phys. **91**, 1 (2016).

[101] G. Eichmann, C. S. Fischer, and H. Sanchis-Alepuz, Light baryons and their excitations, Phys. Rev. D **94**, 094033 (2016).

[102] V. D. Burkert and C. D. Roberts, Colloquium: Roper resonance: Toward a solution to the fifty year puzzle, Rev. Mod. Phys. **91**, 011003 (2019).

[103] C. Chen, Y. Lu, D. Binosi, C. D. Roberts, J. Rodríguez-Quintero, and J. Segovia, Nucleon-to-Roper electromagnetic transition form factors at large $Q^2$, Phys. Rev. D **99**, 034013 (2019).

[104] S.-X. Qin, C. D. Roberts, and S. M. Schmidt, Poincaré-covariant analysis of heavy-quark baryons, Phys. Rev. D **97**, 114017 (2018).

[105] S.-X. Qin, C. D Roberts, and S. M. Schmidt, Spectrum of light- and heavy-baryons, Few Body Syst. **60**, 26 (2019).

[106] C. Chen, G. I. Krein, C. D. Roberts, S. M. Schmidt, and J. Segovia, Spectrum and structure of octet and decuplet baryons and their positive-parity excitations, Phys. Rev. D **100**, 054009 (2019).

[107] Y. Lu, C. Chen, Z.-F. Cui, C. D. Roberts, S. M. Schmidt, J. Segovia, and H. S. Zong, Transition form factors: $\gamma^* + p \to \Delta(1232)$, $\Delta(1600)$, Phys. Rev. D **100**, 034001 (2019).

[108] G. Eichmann, Theory introduction to baryon spectroscopy, in 15th International Conference on the Structure of Baryons, arXiv:2202.13378.

[109] A. J. F. Siegert, Note on the interaction between nuclei and electromagnetic radiation, Phys. Rev. **52**, 787 (1937).

[110] L. Tiator, Pion electroproduction and Siegert's theorem, Few Body Syst. **57**, 1087 (2016).

[111] G. F. Chew, M. L. Goldberger, F. E. Low, and Y. Nambu, Relativistic dispersion relation approach to photomeson production, Phys. Rev. **106**, 1345 (1957).

[112] P. Dennery, Theory of the electro- and photoproduction of $\pi$ mesons, Phys. Rev. **124**, 2000 (1961).

[113] F. A. Berends, A. Donnachie, and D. L. Weaver, Photoproduction and electroproduction of pions. 1. Dispersion relation theory, Nucl. Phys. B **4**, 1 (1967).

[114] C. Ciofi Degli Atti, Electron scattering by nuclei, Prog. Part. Nucl. Phys. **3**, 163 (1978).

[115] D. Rönchen, M. Döring, F. Huang, H. Haberzettl, J. Haidenbauer, C. Hanhart, S. Krewald, U.-G. Meißner, and K. Nakayama, Coupled-channel dynamics in the reactions $\pi N \to \pi N, \eta N, K\Lambda, K\Sigma$, Eur. Phys. J. A **49**, 44 (2013).

[116] M. Döring, C. Hanhart, F. Huang, S. Krewald, and U.-G. Meißner, Analytic properties of the scattering amplitude and resonances parameters in a meson exchange model, Nucl. Phys. A **829**, 170 (2009).

[117] M. Döring, C. Hanhart, F. Huang, S. Krewald, and U.-G. Meißner, The role of the background in the extraction of resonance contributions from meson-baryon scattering, Phys. Lett. B **681**, 26 (2009).

[118] J. Blatt and V. Weisskopf, *Theoretical Nuclear Physics* (John Wiley & Sons, New York, 1952).

[119] D. M. Manley, R. A. Arndt, Y. Goradia, and V. L. Teplitz, An isobar model partial wave analysis of $\pi N \to \pi\pi N$ in the center-of-mass energy range 1320 MeV to 1930 MeV, Phys. Rev. D **30**, 904 (1984).

[120] A. V. Anisovich, R. Beck, E. Klempt, V. A. Nikonov, A. V. Sarantsev, and U. Thoma, Pion- and photo-induced transition amplitudes to $\Lambda K$, $\Sigma K$, and $N\eta$, Eur. Phys. J. A **48**, 88 (2012).

[121] C. Mertz, C. E. Vellidis, R. Alarcon, D. H. Barkhuff, A. M. Bernstein, W. Bertozzi, V. Burkert, J. Chen, J. R. Comfort, G. Dodson, S. Dolfini, K. Dow, M. Farkhondeh, J. M. Finn, S. Gilad, R. W. Gothe, X. Jiang, K. Joo, N. I. Kaloskamis, A. Karabarbounis *et al.*, Search for Quadrupole Strength in the Electroexcitation of the $\Delta(1232)$, Phys. Rev. Lett. **86**, 2963 (2001).

[122] D. Elsner *et al.*, Measurement of the $LT$ asymmetry in $\pi^0$ electroproduction at the energy of the $\Delta(1232)$ resonance, Eur. Phys. J. A **27**, 91 (2006).

[123] K. Joo *et al.* (CLAS Collaboration), Measurement of the polarized structure function sigma(LT-prime) for p(polarized-p, e-prime p) pi0 in the Delta(1232) resonance region, Phys. Rev. C **68**, 032201 (2003).

[124] N. F. Sparveris, R. Alarcon, D. Barkhuff, A. Bernstein, W. Bertozzi, J. Calarco, F. Casagrande, J. Chen, J. Comfort, M. O. Distler, G. Dodson, S. Dolfini, A. Dooley, K. Dow, M. Farkondeh, S. Gilad, R. Hicks, M. Holtrop, A. Hotta, X. Jiang *et al.* (OOPS Collaboration), Measurement of the $R_{\rm LT}$ response function for $\pi^0$ electroproduction at $Q^2 = 0.070(\mathrm{GeV}/c)^2$ in the $\vec{N}\,\Delta$ transition, Phys. Rev. C **67**, 058201 (2003).

[125] J. J. Kelly *et al.* (Jefferson Lab Hall A Collaboration), Recoil Polarization for $\Delta$ Excitation in Pion Electroproduction, Phys. Rev. Lett. **95**, 102001 (2005).

[126] P. Bartsch, D. Baumann, J. Bermuth, R. Bohm, K. Bohinc, D. Bosnar, M. Ding, M. Distler, D. Drechsel, D. Elsner, I. Ewald, J. Friedrich, J. M. Friedrich, S. Grozinger, S. Hedicke, P. Jennewein, M. Kahrau, S. S. Kamalov, F. Klein, K. W. Krygier, A. Liesenfeld *et al.*, Measurement of the Beam-Helicity Asymmetry in the $p(\vec{e}, e'p)\pi^0$ Reaction at the Energy of the $\Delta(1232)$ Resonance, Phys. Rev. Lett. **88**, 142001 (2002).

[127] I. K. Bensafa *et al.* (MAMI-A1 Collaboration), Beam-helicity asymmetry in photon and pion electroproduction in the $\Delta(1232)$ resonance region at $Q^2 = 0.35(\mathrm{GeV}/c)^2$, Eur. Phys. J. A **32**, 69 (2007).

[128] G. Laveissiere *et al.* (JLab Hall A Collaboration), Backward electroproduction of $\pi^0$ mesons on protons in the region of nucleon resonances at four momentum transfer squared $Q^2 = 1.0\,\mathrm{GeV}^2$, Phys. Rev. C **69**, 045203 (2004).

[129] M. Ungaro *et al.* (CLAS Collaboration), Measurement of the $N \to \Delta^+(1232)$ Transition at High Momentum

Transfer by $\pi^0$ Electroproduction, Phys. Rev. Lett. **97**, 112003 (2006).
[130] J. Gayler, Electroproduction of $\pi^0$ mesons in the region of $\Delta(1232)$ with momentum transfer $q^2 = 15\,\mathrm{fm}^{-2}$, DESY Technical Report No. DESY-F21-71-2, 1971 (unpublished).
[131] J. May, Koinzidenzmessungen zur Untersuchung der Reaktion $ep \to ep\pi^0$ beim Impulsübertrag $q^2 \approx 1\,\mathrm{GeV}^2$ im Massenbereich zwischen 1.136 und 1.316 GeV, Ph.D. thesis, Hamburg University, 1971 (unpublished).
[132] C. T. Hill, Higgs Scalars and the nonleptonic weak interactions, Ph.D. thesis, California Institute of Technology, 1977.
[133] K. Joo *et al.* (CLAS Collaboration), $Q^2$ Dependence of Quadrupole Strength in the $\gamma^* p \to \Delta^+(1232) \to p\pi^0$ Transition, Phys. Rev. Lett. **88**, 122001 (2002).
[134] V. V. Frolov, G. S. Adams, A. Ahmidouch, C. S. Armstrong, K. Assamagan, S. Avery, O. K. Baker, P. Bosted, V. Burkert, R. Carlini, R. M. Davidson, J. Dunne, T. Eden, R. Ent, D. Gaskell, P. Gueye, W. Hinton, C. Keppel, W. Kim, M. Klusman *et al.*, Electroproduction of the $\Delta(1232)$ Resonance at High Momentum Transfer, Phys. Rev. Lett. **82**, 45 (1999).
[135] R. Siddle *et al.*, Coincidence $\pi^0$ electroproduction experiments in the first resonance region at momentum transfers of 0.3, 0.45, 0.60, 0.76 GeV/c$^2$, Nucl. Phys. B **35**, 93 (1971).
[136] R. Haidan, Elektroproduktion pseudoskalarer Mesonen im Resonanzgebiet bei großen Impulsüberträgen, Ph.D. thesis, Hamburg University, 1979 (unpublished).
[137] F. Kalleicher, U. Dittmayer, R. W. Gothe, H. Putsch, T. Reichelt, B. Schoch, and M. Wilhelm, The determination of $\sigma_{LT}/\sigma_{TT}$ in electropion production in the $\Delta$ resonance region, Z. Phys. A **359**, 201 (1997).
[138] K. Baetzner *et al.*, $\pi^0$ electroproduction at the $\Delta(1236)$ resonance at a four-momentum transfer of $q^2 = 0.3(\mathrm{GeV}/c)^2$, Nucl. Phys. B **76**, 1 (1974).
[139] A. Latham *et al.*, Coincidence electroproduction of single neutral pions in the resonance region at $q^2 = 0.5(\mathrm{GeV}/c)^2$, Nucl. Phys. B **156**, 58 (1979).
[140] A. Latham *et al.*, Electroproduction of $\pi^0$ mesons in the resonance region at $q^2 = 1.0\,\mathrm{GeV}/c^2$, Nucl. Phys. B **189**, 1 (1981).
[141] S. C. Stave, Lowest $Q^2$ measurement of the $\gamma^* p \to \Delta$ reaction: Probing the pionic contribution, Ph.D. thesis, MIT, 2006 (unpublished).
[142] N. F. Sparveris *et al.*, Determination of quadrupole strengths in the $\gamma^* p \to \Delta(1232)$ transition at $Q^2 = 0.20(\mathrm{GeV}/c)^2$, Phys. Lett. B **651**, 102 (2007).
[143] J. C. Alder, F. W. Brasse, W. Fehrenbach, J. Gayler, S. P. Goel, R. Haidan, V. Korbel, J. May, M. Merkwitz, and A. Nurimba, Electroproduction of neutral pions in the resonance region, Nucl. Phys. B **105**, 253 (1976).
[144] N. G. Afanasev, A. S. Esaulov, A. M. Pilipenko, and Yu. I. Titov, Separation of transversal and longitudinal components of cross-section of pion electroproduction on proton near the threshold, Pisma Zh. Eksp. Teor. Fiz. **22**, 400 (1975).
[145] W. J. Shuttleworth *et al.*, Coincidence $\pi^0$ electroproduction in the second resonance region, Nucl. Phys. B **45**, 428 (1972).
[146] H. Blume, R. Farber, N. Feldmann, K. Heinloth, D. Kramarczyk, F. Kuckelkorn, H. J. Michels, J. Pasler, and J. P. Dowd, Electroproduction of $\pi^0$-mesons on protons at very low values of $|q^2|$, Z. Phys. C **16**, 283 (1983).
[147] M. Rosenberg, Electroproduction of neutral $\pi$ mesons in the range of the two nucleon resonance at 0.3 GeV$^2$/c$^2$ momentum transfer, Master thesis, Bonn University, 1979.
[148] V. Gerhardt, Pion-Elektroproduktion im Bereich der 2. und 3. Nukleonresonanz, Ph.D. thesis, Hamburg University, 1979 (unpublished).
[149] C. Kunz *et al.* (MIT-Bates OOPS Collaboration), Measurement of the transverse longitudinal cross-sections in the $p(e\to, e'p)\pi^0$ reaction in the $\Delta$ region, Phys. Lett. B **564**, 21 (2003).
[150] S. Stave *et al.*, Lowest $Q^2$ measurement of the $\gamma^* p \to \Delta$ Reaction: Probing the pionic contribution, Eur. Phys. J. A **30**, 471 (2006).
[151] N. F. Sparveris, R. Alarcon, A. M. Bernstein, W. Bertozzi, T. Botto, P. Bourgeois, J. Calarco, F. Casagrande, M. O. Distler, K. Dow, M. Farkondeh, S. Georgakopoulos, S. Gilad, R. Hicks, M. Holtrop, A. Hotta, X. Jiang, A. Karabarbounis, J. Kirkpatrick, S. Kowalski *et al.* (OOPS Collaboration), Investigation of the Conjectured Nucleon Deformation at Low Momentum Transfer, Phys. Rev. Lett. **94**, 022003 (2005).
[152] G. A. Warren *et al.* (M.I.T.-Bates OOPS, and FPP Collaborations), Induced proton polarization for $\pi^0$ electroproduction at $Q^2 = 0.126\,\mathrm{GeV}^2/c^2$ around the $\Delta(1232)$ resonance, Phys. Rev. C **58**, 3722 (1998).
[153] T. Pospischil, P. Bartsch, D. Baumann, J. Bermuth, R. Bohm, K. Bohinc, S. Derber, M. Ding, M. Distler, D. Drechsel, D. Elsner, I. Ewald, J. Friedrich, J.M. Friedrich, R. Geiges, S. Hedicke, P. Jennewein, M. Kahrau, S.S. Kamalov, F. Klein *et al.*, Measurement of the Recoil Polarization in the $p(\vec{e}, e'\vec{p})\pi^0$ Reaction at the $\Delta(1232)$ Resonance, Phys. Rev. Lett. **86**, 2959 (2001).
[154] K. Joo *et al.* (CLAS Collaboration), Measurement of the polarized structure function $\sigma_{LT'}$ for $p(\vec{e}, e'\pi^+)n$ in the $\Delta(1232)$ resonance region, Phys. Rev. C **70**, 042201 (2004).
[155] K. Park (private communication).
[156] D. Gaskell *et al.*, Longitudinal Electroproduction of Charged Pions from $^1$H, $^2$H, and $^3$He, Phys. Rev. Lett. **87**, 202301 (2001).
[157] H. Egiyan *et al.* (CLAS Collaboration), Single $\pi^+$ electroproduction on the proton in the first and second resonance regions at $0.25\,\mathrm{GeV}^2 < Q^2 < 0.65\,\mathrm{GeV}^2$, Phys. Rev. C **73**, 025204 (2006).
[158] H. Breuker *et al.*, Forward $pi^+$ electroproduction in the first resonance region at four momentum transfers $q^2 = 0.15(\mathrm{GeV}/c)^2$ and $0.3(\mathrm{GeV}/c)^2$, Nucl. Phys. B **146**, 285 (1978).
[159] G. Bardin, J. Duclos, J. Julien, A. Magnon, B. Michel, and J. C. Montret, A measurement of the longitudinal and transverse parts of the $\pi^+$ electroproduction cross section at 1175 MeV pion-nucleon centre-of-mass energy, Lett. Nuovo Cimento **13**, 485 (1975).
[160] G. Bardin, J. Duclos, A. Magnon, B. Michel, and J. C. Montret, A transverse and longitudinal cross-section separation in a $\pi^+$ electroproduction coincidence experiment and the pion radius, Nucl. Phys. B **120**, 45 (1977).
[161] M. Davenport, Electroproduction of neutral and positive pions between the first and second resonance regions., Ph.D. thesis, Lancaster University, 1980 (unpublished).
[162] O. Vapenikova *et al.*, Electroproduction of single charge d pions from deuterium at $Q^2 \approx 1\,\mathrm{GeV}^2$ in the resonance region, Z. Phys. C **37**, 251 (1988).
[163] J. C. Alder, H. Behrens, F. W. Brasse, W. Fehrenbach, J. Gayler, S. P. Goel, R. Haidan, V. Korbel, J. May, and M.

Merkwitz, Electroproduction of $\pi^+$ mesons in the resonance region, Nucl. Phys. B **99**, 1 (1975).

[164] E. Evangelides *et al.*, Electroproduction of $\pi^+$ mesons in the second and third resonance regions, Nucl. Phys. B **71**, 381 (1974).

[165] H. Breuker *et al.*, Electroproduction of $\pi^+$ mesons at forward and backward direction in the region of the $D_{13}(1520)$ and $F_{15}(1688)$ resonances, Z. Phys. C **13**, 113 (1982).

[166] H. Breuker *et al.*, Backward electroproduction of $\pi^+$ mesons in the second and third nucleon resonance regions, Z. Phys. C **17**, 121 (1983).

[167] C. S. Armstrong, P. Stoler, G. S. Adams, A. Ahmidouch, K. Assamagan, S. Avery, O. K. Baker, P. Bosted, V. Bukert, R. Carlini, J. Dunne, T. Eden, R. Ent, V.V. Frolov, D. Gaskell, P. Gueye, W. Hinton, C. Keppel, W. Kim, M. Klusman *et al.* (Jefferson Lab E94014 Collaboration), Electroproduction of the $S_{11}(1535)$ resonance at high momentum transfer, Phys. Rev. D **60**, 052004 (1999).

[168] H. Denizli *et al.* (CLAS Collaboration), $Q^2$ dependence of the $S_{11}(1535)$ photocoupling and evidence for a $P$-wave resonance in $\eta$ electroproduction, Phys. Rev. C **76**, 015204 (2007).

[169] R. Thompson *et al.* (CLAS Collaboration), The $ep \to e'p\eta$ Reaction at and above the $S_{11}(1535)$ Baryon Resonance, Phys. Rev. Lett. **86**, 1702 (2001).

[170] V. Burkert and Z.-j. Li, What do we know about the $Q^2$ evolution of the Gerasimov-Drell-Hearn sum rule? Phys. Rev. D **47**, 46 (1993).

[171] F. Ravndal, Electroproduction of nucleon resonances in a relativistic quark model, Phys. Rev. D **4**, 1466 (1971).

[172] F. W. Brasse, W. Flauger, J. Gayler, V. Gerhardt, S. P. Goel, C. Gossling, R. Haidan, M. Merkwitz, D. Pock, and H. Wriedt, Separation of $\sigma_L$ and $\sigma_T$ in $\eta$ electroproduction at the resonance $S_{11}(1535)$, Nucl. Phys. B **139**, 37 (1978).

[173] H. Breuker *et al.*, Determination of $R = \sigma_L/\sigma_T$ from $\eta$ electroproduction at the $S_{11}(1535)$ resonance, Phys. Lett. B **74**, 409 (1978).

[174] M. M. Dalton *et al.*, Electroproduction of $\eta$ mesons in the $S_{11}(1535)$ resonance region at high momentum transfer, Phys. Rev. C **80**, 015205 (2009).

[175] George Washington University, SAID website, http://gwdac.phys.gwu.edu, 2021.

[176] J. Gao, L. Harland-Lang, and J. Rojo, The structure of the proton in the LHC precision era, Phys. Rep. **742**, 1 (2018).

[177] R. D. Ball, L. Del Debbio, S. Forte, A. Guffanti, J. I. Latorre, J. Rojo, and M. Ubiali (NNPDF Collaboration), Fitting parton distribution data with multiplicative normalization uncertainties, J. High Energy Phys. 05 (2010) 075.

[178] M. Mai and Ulf-G. Meißner, New insights into antikaon-nucleon scattering and the structure of the $\Lambda(1405)$, Nucl. Phys. A **900**, 51 (2013).

[179] F. James and M. Roos, Minuit - a system for function minimization and analysis of the parameter errors and correlations, Comput. Phys. Commun. **10**, 343 (1975).

[180] JBW Interactive Scattering Analysis website (under development), https://JBW.phys.gwu.edu, 2021.

[181] R. Thompson, Eta electroproduction in the region of the isospin 1/2 1535 MeV baryon resonance, Ph.D. thesis, University of Pittsburgh, 2000 (unpublished).

[182] D. S. Carman *et al.* (CLAS Collaboration), First Measurement of Transferred Polarization in the Exclusive $\vec{e}p \to e'K^+\Lambda$ reaction, Phys. Rev. Lett. **90**, 131804 (2003).

[183] P. Ambrozewicz *et al.* (CLAS Collaboration), Separated structure functions for the exclusive electroproduction of $K^+\Lambda$ and $K^+\Sigma^0$ final states, Phys. Rev. C **75**, 045203 (2007).

[184] R. Nasseripour *et al.* (CLAS Collaboration), Polarized structure function $\sigma_{LT'}$ for $p(\vec{e}, e'K^+)\Lambda$ in the nucleon resonance region, Phys. Rev. C **77**, 065208 (2008).

[185] D. S. Carman *et al.* (CLAS Collaboration), Beam-recoil polarization transfer in the nucleon resonance region in the exclusive $\vec{e}p \to e'K^+\vec{\Lambda}$ and $\vec{e}p \to e'K^+\vec{\Sigma}^0$ reactions at CLAS, Phys. Rev. C **79**, 065205 (2009).

[186] D. S. Carman, K. Park, B. A. Raue, and V. Crede (CLAS Collaboration), Separated structure functions for exclusive $K^+\Lambda$ and $K^+\Sigma^0$ electroproduction at 5.5 GeV with CLAS, Phys. Rev. C **87**, 025204 (2013).

[187] M. Gabrielyan *et al.* (CLAS Collaboration), Induced polarization of $\Lambda(1116)$ in kaon electroproduction, Phys. Rev. C **90**, 035202 (2014).

[188] GWU, Colonial One High Performance Computing, https://colonialone.gwu.edu, 2021.

[189] D. Krause and P. Thörnig, JURECA: Modular supercomputer at Jülich Supercomputing Centre, J. Large Scale Res. Facil. **4**, A132 (2018).